Characterisation of Musculoskeletal Interactions After Spinal Cord Injury

by

Carolyn Rae Maurus

A thesis submitted in partial fulfilment for the
degree of Master of Science

in the
Department of Biomedical Engineering
University of Strathclyde

August 2014

Copyright Declaration

This thesis is the result of the author's original research. It has been composed by the author and has not been previously submitted for examination which has led to the award of a degree.

The copyright of this thesis belongs to the author under the terms of the United Kingdom Copyright Acts as qualified by University of Strathclyde Regulation 3.50. Due acknowledgement must always be made of the use of any material contained in, or derived from, this thesis.

Signed:

Date:

Abstract

A well-established principle called Wolff's Law asserts that the changes in form and/or function of bone are followed by changes in its internal architecture (Frost 1994). Bone is adaptive, and its strength is dependent on its mechanical loading history. The largest loads imposed on bones are generally the result of muscular contraction (Lu et al. 1997), and thus bone adaptation is strongly linked with muscle activity.

Following a complete spinal cord injury (SCI), paralysis of the lower limbs leads to rapid muscle atrophy. In time, this is followed by bone loss due to the extreme reduction in mechanical loading on the previously weight-bearing bones of the lower limbs. This research project aimed to study how early muscle atrophy could be used to predict future bone loss.

Eighteen subjects with motor complete SCI were scanned using peripheral quantitative computed tomography (pQCT) at the 66% distal tibia at four separate time intervals within the first year following injury. Fully automated software was then developed which was able to segment the tissues within each scan, ultimately determining the quantities of fat, muscle, and bone. From these data, changes in tissue volume could be characterised for individual subjects. Over 12 months, fat increased by $39.2\% \pm 42.4$, muscle decreased by $4.4\% \pm 17.3$, and cortical bone decreased by $2.5\% \pm 2.3$. The data further revealed that there was a positive, but weak, correlation between change in muscle CSA at 4 months post-SCI and change in cortical bone CSA at 12 months post-SCI ($r = 0.27$) when compared to the baseline scan; however, this value was not statistically significant.

These results suggest that there may be a relationship between early muscle atrophy and future bone loss. However, future work in this area must be accomplished to support this theory.

Acknowledgements

I would like to use this opportunity to express my gratitude to everyone who supported and helped me throughout the course of this project. In particular, I would like to give my warm thanks to my supervisor Dr. Sylvie Coupaud; you have been an incredible support to me. Thank you for providing me with the opportunity to carry out this project, and encouraging me throughout. Your advice on both this project and my future endeavours have been especially valuable.

In addition, I would like to extend my thanks to the Queen Elizabeth National Spinal Injuries Unit at Southern General Hospital for encouraging the research and providing their support.

I would like to further acknowledge all of the people who lectured in the taught portion of our course at the University of Strathclyde. I gained so much background and knowledge within both medicine and biomedical engineering through these courses, which were essential in developing this project.

Contents

List of Figures

List of Tables

Abbreviations

ASIA	American Spinal Injury Association
BMC	Bone Mineral Content
BMD	Bone Mineral Density
BMI	Body Mass Index
CNS	Central Nervous System
CSA	Cross-Sectional Area
CSV	Comma Separated Values
CT	Computed Tomography
DXA	Dual-Energy X-ray Absorptiometry
FIR	Finite Impulse Response
GUI	Graphical User Interface
HU	Hounsfield Units
MES	Minimally Effective Strains
MRI	Magnetic Resonance Imaging
pQCT	Peripheral Quantitative Computed Tomography
SCI	Spinal Cord Injury
SD	Standard Deviation

Chapter 1

Introduction

1.1 Thesis Organisation

This introductory chapter provides a brief description of the tissues found within the leg (i.e., bone, muscle, and fat), as well discussing some of the differences between healthy tissue and unhealthy tissue. In addition, Chapter 1 defines spinal cord injury and identifies some of the resulting secondary consequences associated with it. In particular, bone loss following paralysis is described, emphasising the need to further explore this complication. In Chapter 2, a literature review will provide an overview on past studies on bone and muscle loss following spinal cord injury. It will also present imaging techniques that are often used in characterising tissue adaptations, discussing which techniques are more suited for individual studies. Chapter 3 is then provided to outline the study aims and objectives.

Chapter 4 lays out the methodology of the study in depth. This includes details on image acquisition of the leg using Peripheral Quantitative Computed Tomography (pQCT). The processing and image analysis tools developed for the pQCT scans are also presented, relying on novel methods of thresholding. These methods ultimately generate the quantities of each tissue within the scan.

In Chapter 5, the results of the image analysis are presented. First, a software verification is performed, assessing the results of using variable thresholds over fixed thresholds for tissue quantification. Subsequently, the data showing the changes in soft tissue and bone is given, along with representative images. This then allows for the capacity of pQCT scans in predicting bone loss to be presented. Chapter 6 provides a discussion on the results. Chapter 7 then briefly summarises the findings and draws conclusions of this study. In addition, this final chapter explores possible directions of future work.

1.2   Muscle

Skeletal muscles function to move the body. When muscles contract, they pull the bone via tendons, producing movement. Depending on where the muscles connect to the bones, a vast variety of actions can be attained, altering the direction, range, power, and speed of the movement. In addition to producing skeletal movement, muscles are useful in maintaining body position, maintaining body temperature, and storing essential amino acid nutrients.

The structure of skeletal muscle can be seen in Figure 1.1. It is composed of several separate layers. The epimysium surrounds the entire muscle, and is composed of a thick layer of collagen fibres. Within the epimysium, the perimysium subdivides each muscle into separate areas. Each of these individual areas contains a bundle of muscle fibres called a fascicle. The deepest layer of connective tissue within the muscle is known as the endomysium. This layer surrounds each individual muscle fibre.
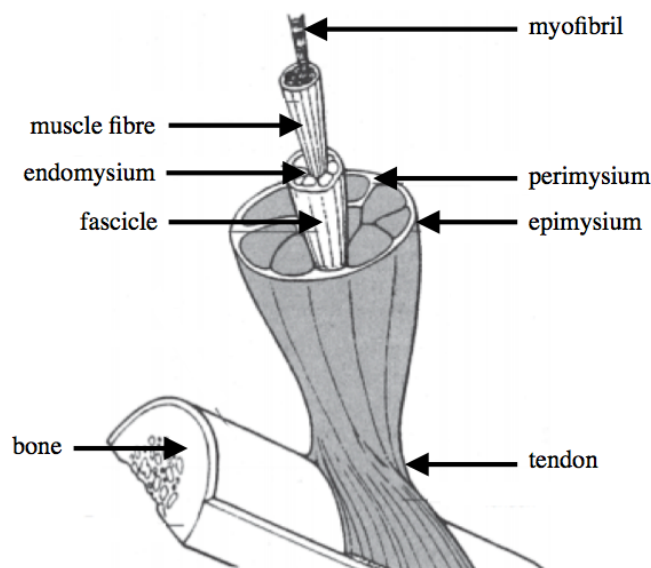
FIGURE 1.1: Skeletal muscle tissue (adapted from Van De Graaff et al. (2010))

Muscle fibres are long and tubular cells and are the main cell unit of muscle tissue. Clusters of cylindrical structures called myofibrils run through each muscle fibre, which are composed of proteins called myofilaments. Myofibrils are capable of extending and contracting, giving the muscle its functionality to provide movement. Muscle fibres also contain stores of glycogen and mitochondria to supply energy to the cells and allow for muscular contraction.

A skeletal muscle begins to contract following stimulation by a motor neuron at a neuromuscular junction. When an action potential arrives, the myofilaments within the muscle fibres begin to interact with each other and the muscle fibres shorten. This contraction produces tension at either end, and the entire skeletal muscle pulls on the tendons at each end, producing musculoskeletal movement. (Van De Graaff et al. 2010)

1.2.1 Muscular Adaptation

Muscle responds rapidly to changes in stimuli. When a muscle falls into disuse, atrophy occurs; contrarily, when a muscle is overused, hypertrophy occurs.

Atrophy is characterised by an overall loss in muscle mass, and can usually be diagnosed through a decrease in size (such as cross-sectional area). Typically, skeletal muscle that does not receive periodic stimulation will lose muscle tone, power, and mass. The condition causes each muscle fibre to become thinner and lose strength. (Martini et al. 2011) Atrophy can be caused by a number of conditions, such as neuromuscular disorders and diseases, ageing, dietary intake, hormonal imbalances, or through immobilisation and disuse (Boonyarom & Inui 2006).

By contrast, muscular hypertrophy is an increase in muscle mass, and can be seen through an increase in size. This occurs when a muscle receives repeated

stimulation near maximum tension. This causes the muscle fibres to develop a higher concentration of mitochondria, enzymes, and glycogen reserves in order to produce energy. As a result, the muscle fibres have more myofibrils than typical muscles, and each myofibril contains more myofilaments. (Martini et al. 2011)

1.3   Bone

The skeletal system has many vital functions within the body. Fundamentally, it makes up the necessary framework to provide support to the body, allowing for movement with the aid of attached muscles. In addition, it provides protection to vital organs, such as the protection of the heart and lungs by the rib cage. Bone also contains red bone marrow, the vital component to haematopoeisis (production of blood cells), in addition to storing calcium within the body. (Martini et al. 2011)

1.3.1   Bone Composition and Structure

1.3.1.1   Bone Shapes

There are typically 206 bones within the adult human skeleton, which are often categorised according to their shape. These categories include flat bones, irregular bones, sesamoid bones, short bones and long bones. Long bones such as the femur and tibia consist of a long shaft known as the diaphysis, the rounded ends called the epiphyses, and the widened, coned-shaped area between the diaphysis and the epiphyses known as the metaphyses. This structure can be seen in Figure 1.2. (Van De Graaff et al. 2010)
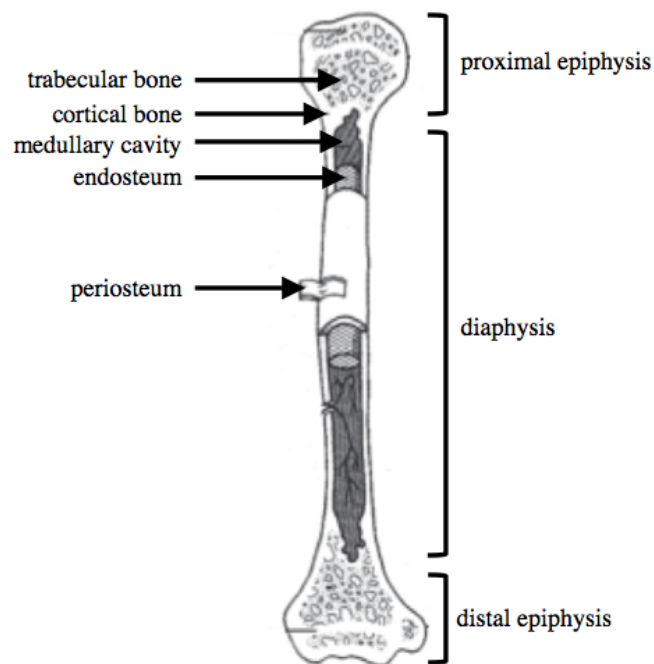
FIGURE 1.2: Long bone structure (adapted from Van De Graaff et al. (2010))

1.3.1.2 Bone as a Composite

Bone is considered a composite material, consisting of both a non-living mineral matrix and living bone cells distributed within the matrix. The bone matrix is composed primarily of inorganic salts such as calcium phosphate and calcium hydroxide, which form crystals of hydroxyapatite, and form nearly two-thirds of the weight of bone. These minerals make the bone strong and able to withstand large forces, but also brittle. Organic Type I collagen fibres are also distributed within the bone matrix, thus ensuring that bone has a higher elasticity and flexibility, and allowing the bones to be better able to withstand bending.

Bone cells make up only approximately 2% of bone, and live within pockets (called lacunae) spread throughout the matrix. There are several different types of cells that are involved in the maintenance of bone structure. Osteocytes are

the primary and most abundant bone cells. These cells are responsible for maintaining mineral homeostasis. They act to release minerals into the circulation. In addition, they regulate bone formation and resorption through stimulating the activity of osteoblasts and osteoclasts. Osteoblasts are cells that produce new bone matrix by making and secreting necessary proteins and other organic compounds. Like osteoblasts, osteoclasts play a critical role in the bone remodelling cycle. Osteoclasts move around to resorb and recycle bone matrix in areas where it is either damaged or inessential. Enzymes and acids produced by osteoclasts act to dissolve the mineral in the matrix and release the stored minerals. The activity of all bone cells results in a dynamic tissue that constantly undergoes remodelling to remove old, microdamaged bone and replace it with new, stronger bone. (Cowin 2001)

1.3.1.3 Cortical Bone

There are two types of bone tissue present within the skeletal system. Both of these types of bone can be found in long bones, as illustrated in Figure 1.2. In long bones, the diaphysis is composed primarily of dense cortical bone, and the epiphyses consist of complex meshworks of trabecular bone surrounded by a thin layer of cortical bone.

Cortical bone, also known as compact bone, is the dense structure that surrounds the bone and the inner marrow. Cortical bone is found primarily on the outer surface of long bones, including throughout the diaphyses, providing the necessary structural support to weight-bearing limbs.

The internal structure of cortical bone is seen in Figure 1.3. The structural units of cortical bone are long cylinders which are known as Haversian systems, or osteons, which are closely packed with one another. Within each Haversian system,

osteocytes are arranged around a central Haversian canal, which contains nerves and blood vessels to supply blood and nutrients to the bone tissue. Concentric cylinders of bone matrix called lamellae surround the Haversian canal. The lacunae containing bone cells are positioned throughout the lamellae.
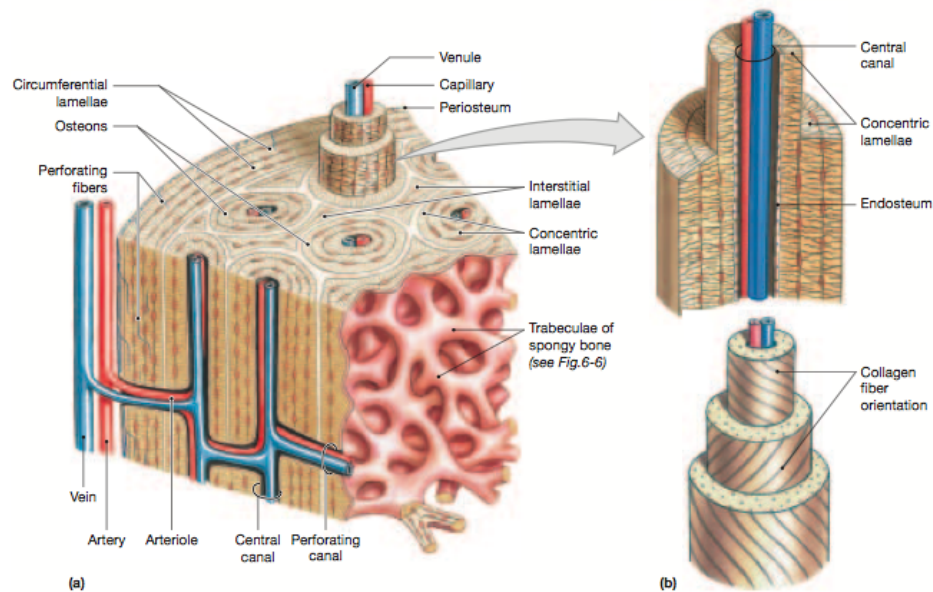
FIGURE 1.3: Cortical bone microstructure (Martini et al. 2011)

All Haversian systems are aligned in the same direction, providing strength in the direction of loading. For example, Haversian systems along the diaphyses of long bones are parallel to the long axis of the shaft, providing high levels of strength when stresses are applied to each end of the bone. However, this configuration is weak when subjected to stresses from the side, and can fracture with relatively small forces. (Cowin 2001)

1.3.1.4 Trabecular Bone

The other type of bone tissue is known as trabecular bone, which is also commonly referred to as cancellous or spongy bone. As illustrated in Figure 1.4, trabecular

bone is porous, with cavities usually filled with red or yellow bone marrow. It is composed of trabeculae, which are thin plates and rods that create the meshwork of trabecular bone. Since there are no blood vessels to carry nutrients to the trabecular bone, nutrients provided from the red bone marrow diffuse across the trabeculae along narrow passageways called canaliculi. Due to the high surface area found in trabecular bone, it is much more highly vascularised than cortical bone, which relies on the narrow Haversian canals to provide nutrients to large amounts of bone.
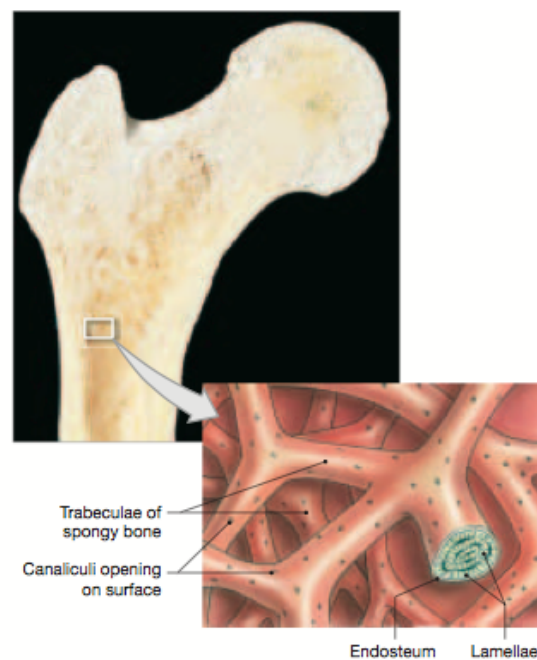
FIGURE 1.4: Trabecular bone microstructure (Martini et al. 2011)

Trabecular bone is found in areas of the skeleton that do not experience high levels of load, or where stresses come from varying directions. The struts of trabecular bone can often be seen arranged along the direction of the applied force to provide greater strength. This type of bone provides several distinct advantages over cortical bone. First, it is able to withstand forces in many directions unlike cortical bone, which is more adapted to uniaxial force. Trabecular bone is also

very light in comparison to cortical bone, making the skeleton lighter. (Cowin 2001)

1.3.1.5 Bone Turnover

Bone remodelling is constantly active in a healthy human skeleton. During the process, a balance occurs between bone matrix deposition and bone resorption by osteoblasts and osteoclasts, respectively. Ideally, the bone cell activity is coupled, functioning such that homeostasis is achieved. In turn, the bone's integrity and strength is maintained.

Several factors can stimulate bone remodelling, including the repair of bone fracture and the regulation of calcium homeostasis within the body. Once bone remodelling is activated, osteoclasts first attach to the bone surface. The cells then begin to resorb the bone matrix through acidification and proteolysis (breakdown of proteins) over the next 2 weeks. Next, a reversal process occurs, where cells appear on the surface of the bone and prepare it for bone deposition by osteoblasts. This process can last as long a 4-5 weeks. During formation, osteoblasts work to replace the bone matrix, continuing for up to 4 months. (Hadjidakis & Androulakis 2006)

1.3.2 Osteoporosis

Osteoporosis is a progressive disease in which bone begins to weaken due to loss in mass and density and increase in porosity. The disease is characterised by the loss of calcium within the bones through a higher rate of osteoclast activity than osteoblast activity. As a bone's calcium is depleted, the bone becomes more brittle and thin. As the bone loses strength, it becomes unable to withstand

normal stresses and is hence more susceptible to fracture. (Bono & Einhorn 2003)

In general, osteoporosis is greatest in trabecular bone regions. Since trabecular bone is more highly vascularised, it responds more quickly and severely to any changes in the body's metabolic system (Bono & Einhorn 2003). A magnified view of healthy trabecular bone and osteoporotic trabecular bone can be seen in Figure 1.5. As the figure indicates, the quantity and thickness of the trabeculae is significantly decreased in the unhealthy bone.
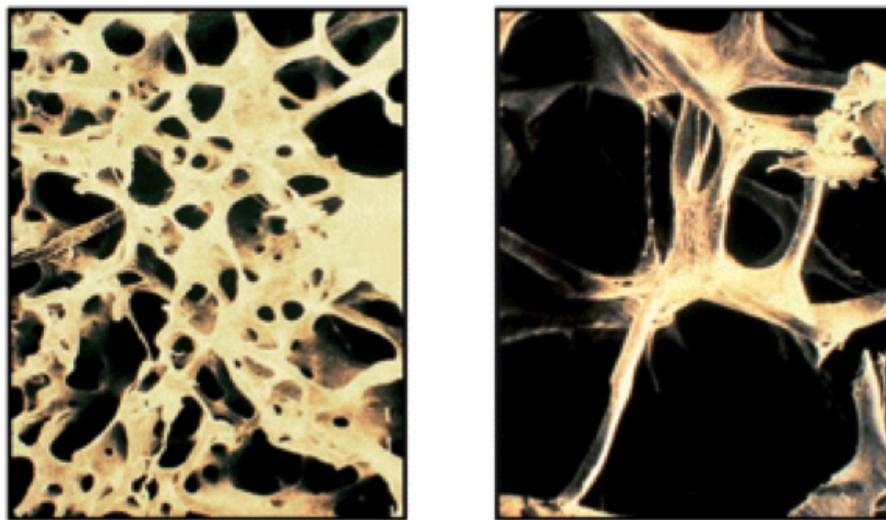
FIGURE 1.5: Differences in trabecular bone microstructure in normal bone (left) and osteoporotic bone (right) (Brandi 2009)

This condition is most often associated with ageing and/or menopause. As an individual ages, their bones' integrity and strength begin to weaken. However, many other different factors can also trigger the onset of osteoporosis. For example, an individual's genetics or hormone levels may increase their risk factor for developing the disease. Poor dietary intake, smoking, or medication use may also contribute to the development of osteoporosis. Accelerated bone loss can also be

seen following disuse due to factors such as paralysis or exposure to microgravity in spaceflight. (National Institutes of Health 2012), (Vico et al. 2000)

1.4 Central Nervous System

The Central Nervous System (CNS) consists of both the brain and the spinal cord. The spinal cord links the brain to the rest of the body, extending from the medulla oblongata near the foramen magnum and down the vertebrae. It stretches through the vertebral canal, a central passageway in the vertebral column.

The vertebral column itself is composed of 33 vertebrae, formed into regions known as the cervical region, the thoracic region, the lumbar region, and the sacral region. The spinal cord can then be divided according to the corresponding region of the vertebral column. There are 31 pairs of spinal nerves that exit the spinal cord: 8 cervical pairs, 12 thoracic pairs, 5 lumbar pairs, 5 sacral pairs, and 1 pair emerging from the cauda equina known as the coccygeal nerve. They are each named according to the vertebrae from which they emerge as seen in Figure 1.6.

A cross-sectional view of the spinal cord shows that it is composed of white and grey matter, as seen in Figure 1.7. White matter contains the tracts which carry sensory and motor information to and from the brain. The deep grey matter is composed of neuronal cell bodies. Extending from each side of the central spinal cord is a dorsal root, which carries sensory information, and a ventral root, which carries motor information. These roots then merge distal to the spinal cord to form the spinal nerve pair of that spinal segment, which carries motor and sensory information. (Martini et al. 2011)
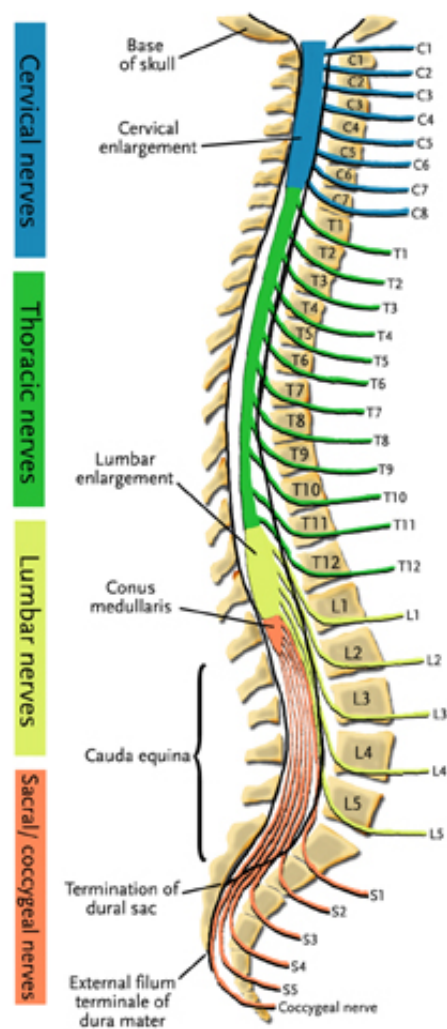
1.4.1   Spinal Cord Injury

A spinal cord injury (SCI) is a traumatic event in which a lesion to the spinal cord, either due to trauma or disease, interrupts the motor and sensory pathways, preventing information from passing from the brain to the rest of the body. As a result, the patient will experience paralysis and loss of sensory information, the extent of which is dependent on the level and completeness of the injury. The
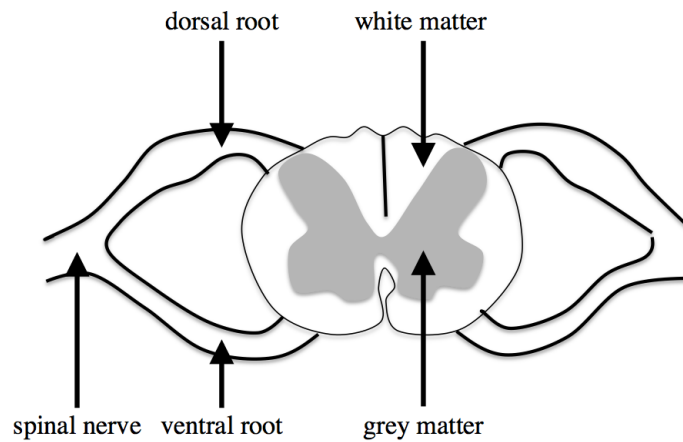
FIGURE 1.7: Cross-sectional view of the spinal cord and spinal nerve roots

neurological levels of a spinal injury are defined by the locations of the spinal nerves (seen in Figure 1.6) where the trauma occurred, occurring at either the cervical, thoracic, lumbar, or sacral region. The higher the location of the lesion to the spinal cord, the greater the extent of impairment to sensory and motor function of the individual.

It is challenging to accurately and consistently classify patients with SCI due to the many different causes and types of injury (Jacobs & Nash 2004). However, standards have been established to uniformly classify patients based on their sensory and motor function. The injury is classified as complete if no sensory or motor function is preserved below the neurological level of the lesion. However, if the injury is incomplete, some motor or sensory pathways are often spared below the level of damage. The completeness of spinal injuries are generally classed using the American Spinal Injury Association (ASIA) Impairment Scale (Table 1.1). The scale classifies the degree of impairment resulting from a spinal cord injury based on both sensory and motor function of the individual, and serves to provide a proper neurological evaluation following a traumatic spinal cord injury. (Maynard et al. 1997)

TABLE 1.1 ASIA Impairment Scale (Maynard et al. 1997)

Class	Completeness	Description
A	Complete	No sensory or motor function is preserved in the sacral segment S4-S5.
B	Incomplete	Sensory but not motor function is preserved below the neurological level and includes the sacral segments S4-S5.
C	Incomplete	Motor function is preserved below the neurological level, and more than half of key muscles below the neurological level have a muscle grade less than 3.
D	Incomplete	Motor function is preserved below the neurological level, and at least half of key muscles below the neurological level have a muscle grade of 3 or more.
E	Normal	Sensory and motor function is normal.

Patients with SCI can be further classified as either paraplegic or tetraplegic. Complete thoracic, lumbar, or sacral spinal injuries generally result in paraplegia, in which function in the lower limbs, pelvis, and/or trunk may be impaired while the upper limbs retain functionality. Higher levels of injury sustained to the cervical region result in tetraplegia (also known as quadriplegia), in which there is a loss in function to both the upper and lower limbs, the pelvis, and the trunk. (Jacobs & Nash 2004)

1.4.1.1 Spastic vs. Flaccid Paralysis

SCI can be further differentiated into patients who have sustained an upper motor neuron lesion or a lower motor neuron lesion. Lesions to the upper motor neuron result in spastic paralysis. In spastic paralysis, muscles in the affected limbs have high tone and often display involuntary movements, spasms, and exaggerated tendon reflexes. This is because the sensory, motor, and autonomic reflexes in the body remain undamaged below the level of injury, despite no longer being controlled by the brain.

In contrast, lesions to the lower motor neuron result in denervation and flaccid paralysis, wherein muscles are limp and weak with no spasms or other muscular movement present. In these scenarios, the patient has lost all sensory and motor reflexes below the level of injury. (Jacobs & Nash 2004)

1.4.1.2 Occurrence of Spinal Cord Injury

Spinal cord injury has a high incidence of morbidity and mortality throughout the world. Although modern medical care has reduced incidences of morbidity and mortality, it is still a particularly devastating life event. Some of the primary causes of SCI include motor vehicle accidents, falls, violence, and sporting injuries (Centers for Disease Control and Prevention 2010).

Throughout the world, the estimated SCI incidence is between 10.4 and 83 cases per million per year (Wyndaele & Wyndaele 2006). Within the United States alone, 200,000 people are currently living with a spinal injury, with up to 15-40 new cases per million people occurring annually (Centers for Disease Control and Prevention 2010). It is estimated that 50-70% of spinal injuries occur in young individuals between the ages of 15 to 35 years, with an average age of 33 years old. Further epidemiological studies indicate that men are at a much higher risk for SCI, with an incidence rate of 3.8/1 in favour of men (Wyndaele & Wyndaele 2006).

1.4.1.3 Consequences of Spinal Cord Injury

As discussed previously, the primary effects of SCI are the loss of sensory and motor function below the level of the lesion. Due to the loss of limb function, the individual may require the use of care givers to provide day-to-day living support, especially in cases of tetraplegia. Additional secondary complications can arise

from SCI as well, that often lead to rehospitalisation of SCI patients. In general, these secondary complications are more severe in tetraplegia than paraplegia. These complications include respiratory distress, pressure ulcers, reduced bladder and bowel function, and cardiovascular disease.

Due to the complete disuse of paralysed limbs and associated lack of physical activity, one of the principle secondary effects of paraplegia or tetraplegia is the rapid muscular atrophy and reduced bone integrity in the affected limbs. Patients with SCI endure osteoporosis following injury, leaving them more susceptible to fracture. (McKinley et al. 1999)

Chapter 2

Literature Review

2.1 Mechanostat Theory

A well-established principle called Wolff's Law asserts that the changes in form and/or function of bone are followed by changes in its internal architecture (Frost 1994). From this theory established in 19th century, Frost expanded this idea to a principle called the Mechanostat theory. The Mechanostat theory is a model that describes bone growth and bone loss as a function of mechanical loading. It was first developed by Harold Frost in the Utah Paradigm of Skeletal Physiology (Frost 2004). This theory proposes that mechanical loading is the dominant factor in bone remodelling. Other factors, such as nutritional intake or hormones, are only secondary modulators of bone strength.

The Mechanostat theory is described by a feedback loop. Increased mechanical strains result in increased bone formation, whereas a decrease in mechanical strains imposed on the bone will result in bone loss. A simplified scheme adapted from Frost's hypothesis can be seen in Figure 2.1.
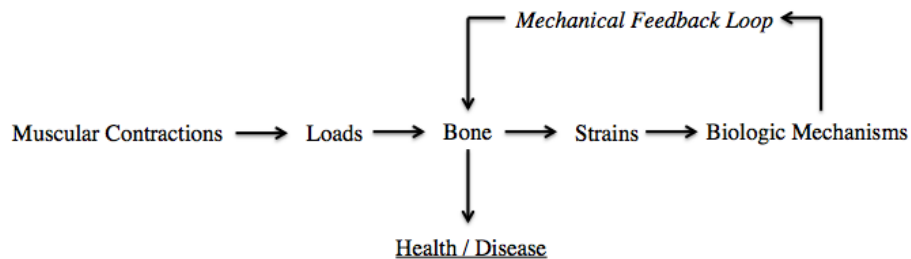
FIGURE 2.1: Simplified mechanostat feedback mechanism (adapted from Frost (2004))

This Mechanostat feedback mechanism can be more clearly visualised through Figure 2.2, which illustrates the Minimally Effective Strains (MES) that lead to remodelling, modelling, and cortical bone microdamage. The line at the bottom of the diagram indicates bone strain thresholds, extending from zero strain on the

left, to bone fracture (F_x) on the right. The vertical axis indicates the level of bone turnover occurring. When bone turnover is negative, the bone is experiencing increased bone resorption, bone loss is occurring, and the bone is weakened. When bone turnover is positive, the bone is experiencing increased osteoblast activity and the bone is strengthened. Neutral bone turnover indicates the bone is maintaining a balance between bone resorption and bone formation, leading to no net change in its strength.

When the strains imposed on the bone fall below a minimum threshold, bone loss occurs. This is defined by the disuse threshold, MES_y. As mechanical strain loading is increased to the maintenance threshold, MES_m, the bone's integrity remains constant. If strains increase past the maintenance threshold but remain less than the damage threshold, MES_p, the bone is strengthened. Loads greater than the damage threshold result in microdamage to the cortical bone. (Frost 2004)
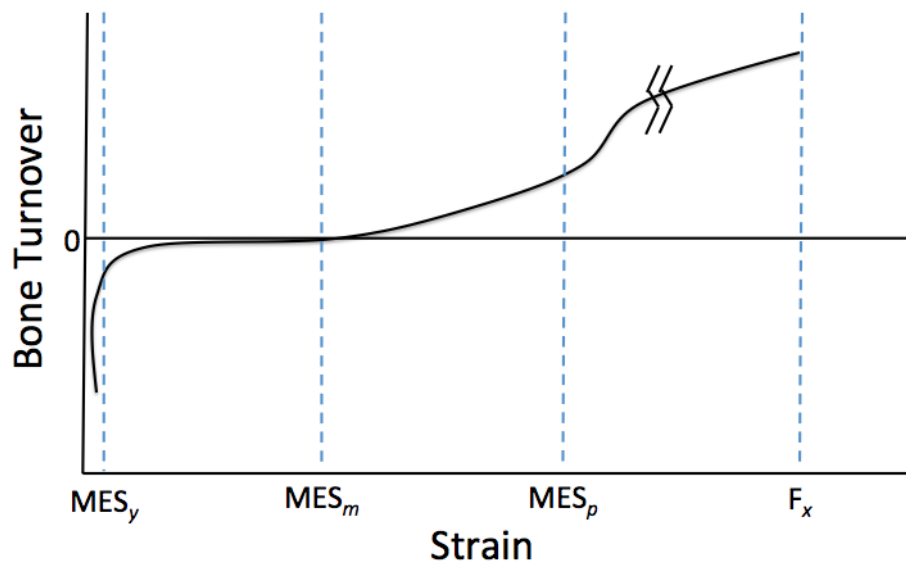
FIGURE 2.2: Modelling, remodelling, and microdamage effects of mechanical strains on bone (adapted from Frost (2004))

2.1.1 Disuse Osteoporosis

As discussed in the previous chapter, multiple factors can lead to osteoporosis. One common cause of bone loss is characterised as disuse osteoporosis, caused by a significant reduction in mechanical loading on the bone. This condition is often a result of bed rest, microgravity, or localised immobilisation of the limbs due to SCI. The ultimate result of mechanical unloading is an increased bone resorption mediated by osteoclasts and an inhibition of osteoblast activity involved in bone formation. In general, disuse osteoporosis results in a thinner cortical shell and coarsened trabeculae (Takata & Yasui 2001).

Bones that are primarily composed of trabecular bone are especially susceptible to disuse osteoporosis. Trabecular bone is much more highly vascularised than cortical bone due to its greater surface area. Therefore, it responds more quickly to any changes in bone metabolism, and changes in mechanical loading results in more prominent bone loss in trabecular regions (Takata & Yasui 2001).

Disuse osteoporosis has also been found to vary dependent on the region of the body. In general, bone loss is most severe in the lower limbs. In a healthy individual, these bones are typically loaded throughout the day as the person moves and ambulates. This loading is achieved through a combination of ground reaction forces, muscular contractions, and static weight-bearing loading (Lau & Guo 2011). Loading is then lost in the case of complete SCI, and in other forms of immobilisation or disuse.

Disuse osteoporosis can be clinically indicated through several means. One such method is through the use of imaging techniques such as Computed Tomography (CT) or Dual-Energy X-ray Absorptiometry (DXA), which are able to accurately estimate bone mineral density (BMD) *in vivo*. Using these measurements, a reduction in BMD is often used as an indicator for osteoporosis.

2.2 Musculoskeletal Interactions

As discussed in Section 2.1.1, one of the loading mechanisms of bone is the contraction of surrounding muscles. When external loads are applied to the limb, muscles transmit high levels of tensile forces to the bone (Lu et al. 1997). This muscular contraction accounts for one of the largest levels of forces on the bone itself. To illustrate these musculoskeletal interactions, Figure 2.3 shows how the muscular contraction of the biceps brachii muscle introduces a load onto the humerus, radius, and ulna bones of the arm.
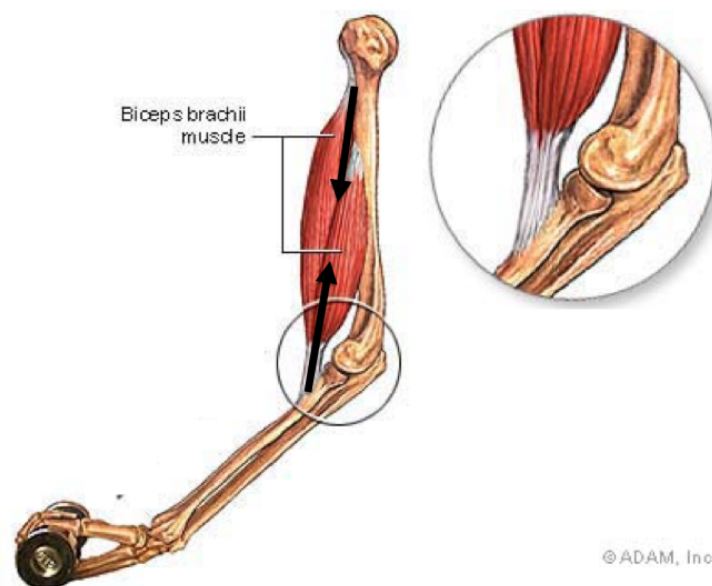
FIGURE 2.3: Musculoskeletal interactions between the biceps brachii muscle and the radius and ulna (adapted from A.D.A.M., Inc. (2013))

Because bone integrity is so dependent on muscular contractions, the health of the muscles can often be used as an indicator of bone strength (Takata & Yasui 2001). Several studies have found a statistically significant positive correlation between BMD and the strength of the proximal muscle group. In a study performed by Calmels et al. (1995), a high correlation existed between the isokinetic muscle

strength of the knee flexors and femoral BMD. Similar relationships were also found in other anatomical regions of the body: correlations have been discovered between the muscle strength of the hip abductors and flexors and the BMD of the femoral neck (Zimmermann et al. 1990), as well as between the muscle strength of the back extensors and BMD of the lumbar spine (Sinaki et al. 1986).

2.3 Tissue Changes Following Spinal Cord Injury

2.3.1 Changes in Muscle

Muscle begins to atrophy quickly following complete paralysis of the lower limbs, beginning within four hours of hospitalisation (Kasper et al. 2002). The level of atrophy in a patient is dependent on the usage of the muscles prior to disuse. Antigravity muscles (i.e., muscles that prevent the body from "falling over" due to gravity) tend to experience exceptionally large levels of atrophy (MacIntosh et al. 2005), whereas their antagonist muscles show a reduced overall level of atrophy.

It is difficult to determine exactly how quickly and severely muscle begins to atrophy following paralysis, as patients are often not clinically stable enough to scan until weeks following their injury. Castro et al. (1999) completed a study characterising muscle loss within six months following a complete spinal injury. However, they noted that the first scan was not completed until after the patients were clinically stable following their injury, which was on average six weeks post-SCI. They observed that average muscle cross-sectional area (CSA) of the leg and thigh was up to 45% smaller in these patients than the able-bodied control group. This suggests a high likelihood that muscle begins to atrophy rapidly following

paralysis. Within the 18-week study period, the *m.* gastrocnemius CSA had reduced by 24%, and the *m.* soleus had reduced by 12% (Castro et al. 1999).

There is a smaller decrease in muscle mass in patients with spastic paralysis due to some level of involuntary muscle activity (Wilmet et al. 1995). As a result, patients with flaccid paralysis experience the most severe muscle loss (Coupaud et al. 2009). A separate study found that SCI subjects with a high level of spasticity had, on average, a 40% greater muscle CSA than subjects with fully flaccid paralysis (Eser, Frotzler, Zehnder, Schiessl & Denoth 2005).

It is possible to use muscular CSA as a direct correlation to and surrogate measure of the muscle's strength, providing quantification of the muscle's potential force generation (Rittweger et al. 2000), (Schantz et al. 1983).

2.3.2 Changes in Fat

Fat exists in many areas throughout the body, and is typically classified as subcutaneous fat or intramuscular fat. In general, fat content tends to increase in the lower limbs following paralysis (Wilmet et al. 1995), both subcutaneously as well as through muscle infiltration in the form of intramuscular fat.

Intramuscular fat has been found to be especially prevalent in patients following a complete SCI. When this occurs, fat infiltrates into individual muscle groups, and thus correlates strongly to muscular atrophy (Gorgey & Dudley 2006). A study by Gorgey & Dudley (2006) found that, 3 months post-injury, intramuscular fat in the thigh had increased by 26%. In a separate study, subjects with SCI had three times more intramuscular fat and four times more subcutaneous fat than the able-bodied control group in the thigh (Elder et al. 2004).

Since intramuscular fat levels increase so drastically over a short time period post-SCI, it is necessary to account and correct for it when considering muscle size. Neglecting this effect can lead to a gross overestimation of muscle size and strength (Elder et al. 2004).

2.3.3 Changes in Bone

Bone loss does not occur as rapidly as muscular atrophy following lower limb paralysis. Although muscle loss can be quantified in as little as days, bone loss does not begin to appear until months afterwards.

Bone loss in trabecular regions of the skeleton is much more rapid and extensive than loss in cortical bone (Wilmet et al. 1995). Following paralysis of the lower limbs, Biering-Sorensen et al. (1990) found a loss in BMC of the proximal tibia (which is rich in trabecular bone) reached a steady-state value of 40-50% after 18-months. Conversely, the femoral shaft (which is primarily cortical bone) had a BMC loss of approximately 20% at 18-months, which continued to decrease linearly thereafter.

Although the trabecular bone sees a reduction in BMD, the cortical shell in long bones appear to retain the same density (although there may be a transient decrease). The reduction in strength of the cortical bone comes from a thinning of the shell (Eser et al. 2004). The study completed by Eser et al. (2004) showed that the cortical CSA is approximately 30% less than normal in the femur and tibia in chronic SCI, most likely due to endosteal resorption, while sustaining the same outer diameter.

As discussed in Section 2.3.1, patients who experience flaccid paralysis tend to have increased levels of muscle atrophy than those who experience spastic paralysis. Coupaud et al. (2009) found that a linear relationship exists between bone

CSA and muscle CSA, and subjects with flaccid SCI were seen to have the smallest muscle and bone size overall, in addition to lower trabecular BMD.

2.3.3.1   Fracture Risk

Due to loss in BMC following SCI, bones become increasingly fragile, increasing the risk of fracture. Vestergaard et al. (1998) found that the risk of fracture doubles in patients who have sustained a spinal injury (2% fracture rate in patients, 1% fracture rate in controls). However, a study by Lazo et al. (2001) reported that up to 34% of SCI patients had a history of fracture. These fractures are especially prevalent as low-energy fractures of the lower extremities (Vestergaard et al. 1998). Often these fractures occur from minor events such as transferring from chair to vehicle or bed, or being turned in bed (Freehafer et al. 1981).

In addition to the increased frequency of fractures, there are several problems that arise in treating lower limb fractures in patients with spinal injury as opposed to the normal population, such as osteomyelitis and pressure sores (Freehafer et al. 1981). Thus treatment methodology must vary from traditional treatment of fractures to accommodate the unusual difficulties presented in paralysed patients.

There has been significant interest in characterising bone loss in SCI patients, and determining a patient's risk for developing a fracture. Fracture risk has been found to directly correlate to BMD (Lazo et al. 2001), (Bartl & Frisch 2009), indicating that BMD measurements can be a significant predictor in the development of fracture in patients with spinal injury. Eser, Frotzler, Zehnder & Denoth (2005) found that tibial fractures most commonly occurred in SCI patients with a BMD of less than 72 mg/cm^3, which was seen in approximately two-thirds of subjects with chronic SCI.

Several possible methods can be used to measure BMD *in vivo* to assess the risk of fracture, which are outlined in the following section.

2.4 Measuring Bone and Tissue Composition *in vivo*

There are several non-invasive methods of measuring bone and tissue composition *in vivo*. Ideally, the method should provide accurate quantification of the bone by calculating true volumetric BMD, in addition to providing differentiation of soft tissue. As a result, imaging outcome measures are used as indicators for both bone and muscle strength.

2.4.1 Dual-Energy X-ray Absorptiometry

Dual-Energy X-ray Absorptiometry (DXA) is currently the gold standard for routine clinical bone densitometry in the diagnosis of osteoporosis (Giangregorio & McCartney 2006), and for assessing risk of fracture in a patient (Tucker et al. 2007). During these clinical evaluations, central DXA is used to scan the lumbar spine and hip in order to calculate projected area BMD.

During the scan, two X-ray beams of different strength are passed through a specific part of the body. The radiation is then absorbed by the bone and soft tissue in different proportions, leaving the remaining radiation energy to pass through the body (Bartl & Frisch 2009). The reduction in X-ray beam energy is then detected, and the contribution of the bone and tissue components can then be calculated to assess the quantities of each. DXA measures projected areal

bone mineral density. In other words, it refers to the amount of bone mineral and soft tissue in a given two-dimensional unit area, measured in g/cm^2.

There are several advantages to DXA over other scanning techniques, making it the most widely used in clinical settings. It has a relatively short scan time, lasting only 5 to 10 minutes for a central DXA (Bartl & Frisch 2009). DXA delivers a low radiation dose to the patient, approximately 1 to 3 μSv (Bartl & Frisch 2009). In general, DXA has an acceptable level of measurement precision (Blake & Fogelman 2007), with an estimated accuracy error of 1-10% and precision of 1% (Bartl & Frisch 2009). In turn, this allows for more accurate diagnoses of patients as well more useful data regarding follow-up and monitoring of osteoporotic progression. However, the precision of DXA has been found to decline with increasing body mass index (BMI) (Yu et al. 2012), indicating that changes in fat mass over time may affect the technique's ability to accurately measure BMD *in vivo*. A study by Bolotin (2007) has found that alterations in tissue composition may affect the accuracy of BMD measurements by as much as 20%. This is because DXA assumes X-rays are being transmitted through two tissue types, bone and soft tissue, and does not take into account any differences in densities in soft tissue, such as that found between fat and muscle. Thus, DXA is not be ideal in tracking BMD in patients who are expected to experience changes in tissue volume, as is the case in SCI.

Another drawback of DXA is that this approach does not consider the material properties of the tissue or its geometric bone distribution (Hudelmaier et al. 2004), and it is therefore not a true volumetric measure of BMD. Since it can not distinguish between cortical and trabecular bone, it is often difficult to detect changes in bone over time, which is critical in characterising rapid bone loss following paralysis.

2.4.2 Peripheral Quantitative Computed Tomography

Quantitative Computed Tomography (QCT) is an alternative non-invasive technique, and differs from other methods such as DXA by creating images showing three-dimensional volumetric BMD measured in g/cm^3. This has the unique advantage in providing quantitative differentiation between cortical and trabecular bone (Bonnick & Lewis 2006). It is especially advantageous in quantifying changes in bone and soft tissue over time, as changes in soft tissue do not lead to the undesired artefacts that affect DXA scans. QCT has been found to be exceptionally accurate in quantifying skeletal muscle (Mitsiopoulos et al. 1998); however, it loses some degree of accuracy when assessing the lipid content within muscle (Schick et al. 2002).

Traditional QCT is mostly used to provide BMD measurements of the spine and appendicular skeleton (Bartl & Frisch 2009). However, the scan exposes the patient to high levels of radiation, approximately 100-1000 mSV. Peripheral QCT (pQCT) is a low-cost, specialised type of QCT. It is smaller than traditional QCT and is utilised to investigate the peripheral skeleton, such as the femur and tibia. This method also provides a much smaller radiation dosage on the order of 1.5 μSv (Braun et al. 1998).

A pQCT scanner can output in several different formats, the most descriptive of which is an array of CT numbers. Each pixel in this array represents a three-dimensional volume, and is known as a voxel. The CT number, which is measured in Hounsfield Units (HUs) represents the attenuation coefficient of the medium in comparison to either water or fat (Engelke et al. 2008). These values can then be converted into BMD, which is based on a linear calibration of the pQCT scanner. Each scanner has a specific calibration equation allowing conversions between HU and g/cm^3.

2.4.3 Magnetic Resonance Imaging

Magnetic Resonance Imaging (MRI) is a method of looking inside the body without the use of ionising X-rays. This technique uses the physics of magnetism and radio waves in order to generate clear images of tissues and structures of human anatomy. In principle, any body tissue that contains hydrogen atoms (most often in the form of water, H_2O) are manipulated to emit a radio signal, which is then detected by the scanner, outputting a clear, high contrast image (Mikla & Mikla 2013).

MRI is especially suited for imaging of soft tissue, and is able to detect even small differences in tissue types and densities. It has been found to have a high level of reproducibility when investigating skeletal muscle, and is reliable in segmenting high-intensity fat, mid-intensity muscle, and low-intensity bone in two-dimensional MRI image slices (Gorgey & Dudley 2006). MRI techniques also exist that provide the quantification of lipid content within muscle (Schick et al. 2002). Despite these advantages, however, it does not provide the same level of detail of bone as X-ray based imaging techniques such as DXA and QCT (Mikla & Mikla 2013). To detect bone structure in MRI, the machine detects the lipids, bone marrow, and water within the porous sections of bone, generating an image of the interstitial space within the bones (Hong et al. 2000). To then determine the BMD and cross-sectional bone geometry, it must be assumed that bone has constant tissue properties across all subjects.

2.4.4 Ultrasound

Ultrasound is a very low-cost, portable, and non-invasive medical imaging technique. This technology is based on sound pulses and echoes. A transducer emits an ultrasound into the tissue. As the ultrasound travels through the tissue and

interacts with the different types of tissue, some of the sound is directed back to the transducer. Based on the timing between the ultrasound emission and its returning echo, an image can be formed showing the tissue structure (Mikla & Mikla 2013).

Quantitative ultrasound can also be used to image bone. In this technique, the transducer and receiver are placed on either side of the patient's bone while the patient's heel is placed in a water bath. From the data obtained through this technique, bone properties can be deduced. However, this technique cannot be used to diagnose osteoporosis (National Osteoporosis Society 2013).

Because ultrasound is highly portable and readily-available, it can be used to measure soft tissue (specifically muscle) early-on following a SCI. In addition, it is an inherently safe technique. As a result, it is often the most ideal imaging technique of measuring tissue in SCI patient to establish a baseline muscle quantity.

Chapter 3

Study Aims and Objectives

The main objective of this project is to characterise the relationships between muscle loss and bone loss following disuse. To accomplish this, cross-sectional images of the leg of a number of paraplegic patients were obtained. These patients were followed during the first year after spinal cord injury, yielding data on tissue changes following immobilisation. From these data, relationships between muscle loss and bone loss could be quantified following the development of novel image processing techniques.

An understanding of these musculoskeletal interactions could yield a predictive capacity in early pQCT scans following a SCI. If there is a useful interrelationship between early muscle loss following paralysis and future bone loss, interventions could be tailored to each specific patient in a preventative manner, with the aim of minimising osteoporosis and bone fracture risk in the future.

Chapter 4

Materials and Methodology

As explained in Chapter 2, a link exists between muscular activity and bone remodelling. In this study, image analysis was used to attempt to establish a definitive relationship between muscular and bone adaptation. This was accomplished through a series of pQCT scans of the lower leg taken from a number of subjects throughout the first year following SCI. These scans were analysed using custom image processing techniques, which were able to differentiate between bone and soft tissue and identify the quantities of each. Ultimately this analysis would establish relationships between muscle loss and bone loss due to immobilisation of the lower limbs.

This chapter first provides a brief introduction on how the pQCT images are obtained. It will then focus on image pre-processing, which allows the images to be analysed in depth by separating the leg from any miscellaneous structures around the body. Following these steps, the images are then segmented, differentiating fat, muscle, bone, and cortical bone through novel thresholding techniques.

4.1 Subjects

Data from eighteen subjects were used in this study, ranging in age from 16 to 72 years. Datasets from an additional eight subjects were excluded from this study due to incomplete data. Each subject sustained a SCI at neurological level L1 or above, resulting in motor-complete paralysis (grade A or B on the ASIA Impairment Scale). Paralysis was either flaccid ($n = 3$) or spastic ($n = 15$).

The study (Longitudinal study of bone demineralisation following spinal cord injury, using peripheral Quantitative Computed Tomography (pQCT)) from which these scan images were released for this project was approved by the South Glasgow & Clyde Research Ethics Committee (REC reference number 05/S0702/131).

Prior to participation in the study, all subjects provided their informed consent in line with the Declaration of Helsinki.

4.2 Image Acquisition

Images were obtained using pQCT. The scans were acquired by Dr. Sylvie Coupaud using a Stratec XCT 3000 scanner (Figure 4.1) at the Queen Elizabeth National Spinal Injuries Unit at Southern General Hospital in Glasgow.

FIGURE 4.1: Stratec XCT 3000 pQCT scanner (image courtesy of Dr. Sylvie Coupaud)

As seen in Figure 4.1, the patient is transferred to a bed while the lower limb is extended and positioned within the scanner during the procedure. The position of the leg within the scanner is a function of the percent distance from the distal tibia, where the length of the patient's tibia is measured as the distance between

the medial joint cleft and the distal end of the medial malleolus. In this study, the slice of interest was located at 66% distal tibia (i.e., a distance of 66% of the total length of the tibia from the distal tibial epiphysis) as seen in Figure 4.2, with a voxel size of 0.5 mm x 0.5 mm x 2 mm. This location was chosen due to its approximate representation of the section with the largest muscle cross-sectional area (Schiessl & Willnecker 1998).
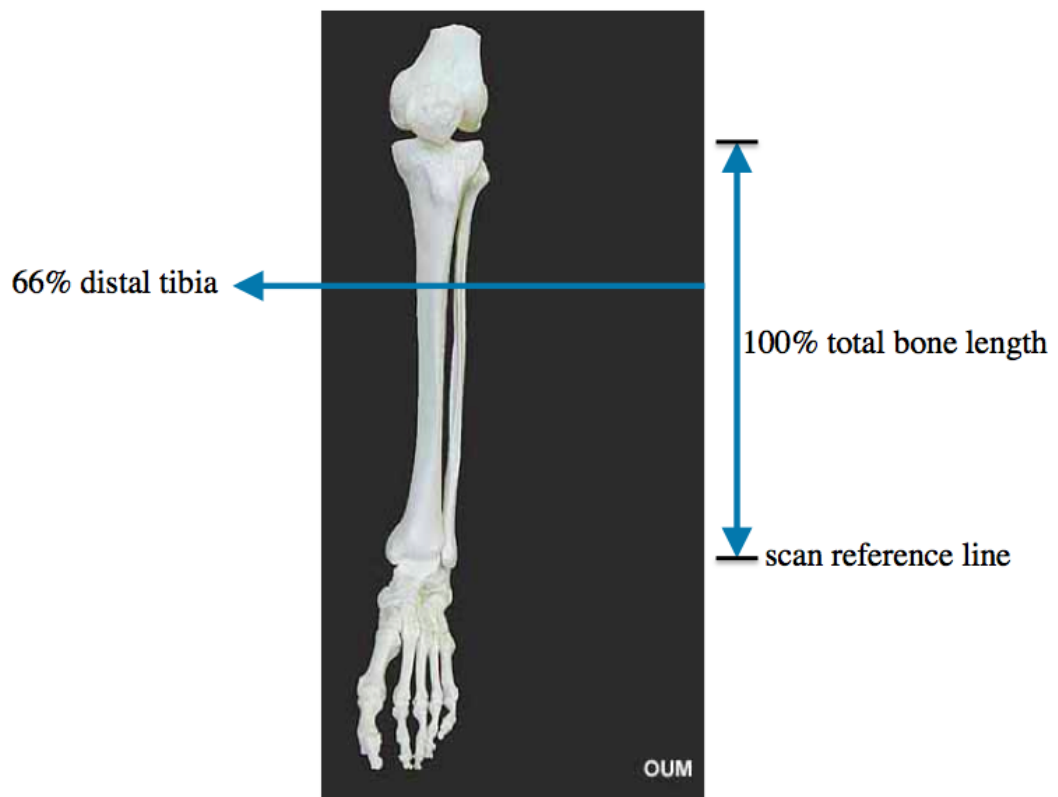

FIGURE 4.2: Diagram of the lower leg illustrating approximate scan location through the tibia and fibula

The reproducibility of the Stratec XCT 3000 was studied by Eser et al. (2004). For most parameters, the reproducibility was better than 1%. For tibial scans, the coefficients of variation ranged from 0.30% (BMD of cortical bone in the diaphysis) to 2.23% (BMD of trabecular bone in the epiphysis).

Scans for each subject were completed at four different time intervals following injury, which were approximately defined by the timescale referenced in Table 4.1. The location of the scan was held consistent, allowing comparison of the obtained images over time.

TABLE 4.1 Approximate pQCT scan times following SCI

Nomenclature	Time Post-SCI
Baseline Scan	1 month
T2 Scan	4 months
T3 Scan	8 months
T4 Scan	12 months

Each cross-sectional image was then exported from the scanner as CSV (comma separated values) files for further analysis.

4.3 Density Conversion

The attenuation values in HUs of each voxel can be converted into bone density values. The scanner is calibrated using a standard phantom manufactured with a bone-equivalent calcium hydroxyapatite material. This allows a linear conversion equation to be used to convert the image from HUs to hydroxyapatite densities in mg/cm^3, which is provided by the manufacturer (Findlay 2012).

$$BMDIm = (HUIm \times 1.495) - 341 \tag{4.1}$$

where $BMDIm$ is the image in mg/cm^3, and $HUIm$ is the image in HUs. This equation has the ability to convert each voxel into a hydroxyapatite equivalent density. Unlike comparable pQCT scanners, the Stratec XCT 3000 is calibrated with respect to fat which is set at 0 mg hydroxyapatite, giving rise to a water density of 60 mg hydroxyapatite.

4.4 Image Pre-Processing

The cross-sectional pQCT images of the lower leg were analysed using Matlab 2014a (The Mathworks, Inc., Natick, Massachusetts, United States), and its associated image processing toolbox. To begin image analysis of each pQCT scan, each CSV file was imported into Matlab. In this format, data is stored within a two-dimensional arrangement of numbers known as an image matrix, where each value in the table represents the CT number of one voxel within the image in HUs (see Figure 4.3).
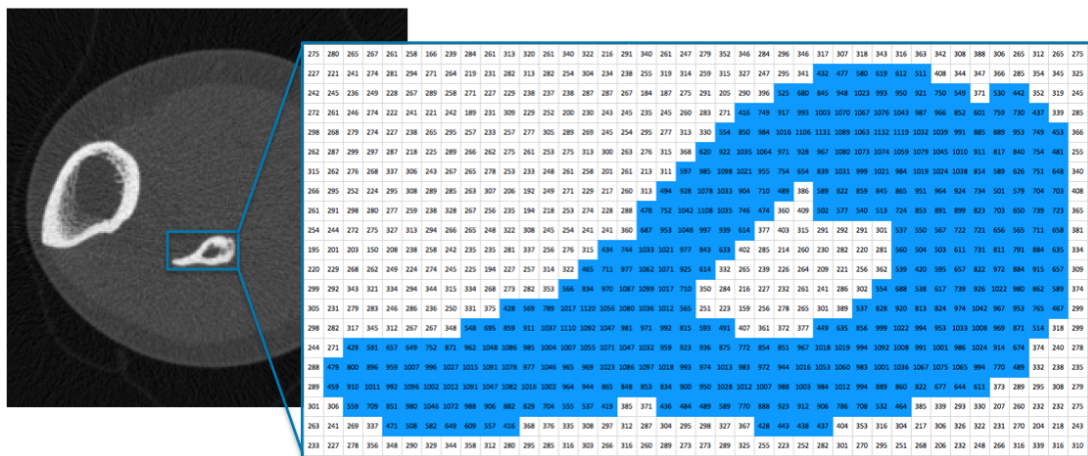

FIGURE 4.3: Image showing matrix representation of voxels

The files were then converted into a greyscale image, which linearly converts each value in the file to a range of 0.0 to 1.0. The minimum density voxel was given a value of 0.0 which corresponded to black, and the maximum density voxel was given a value of 1.0 which corresponded to white. All other values fell in between these intensities. This conversion allows Matlab to output the original image. These intensity values could then be easily converted to hydroxyapatite equivalent densities and HUs where necessary.

In order to analyse the images, the scans needed to be cleaned up to remove the air and any extraneous objects around the leg. Many of the images contained miscellaneous artefacts such as clothing and urine bags, such as that seen in Figure 4.4(a).
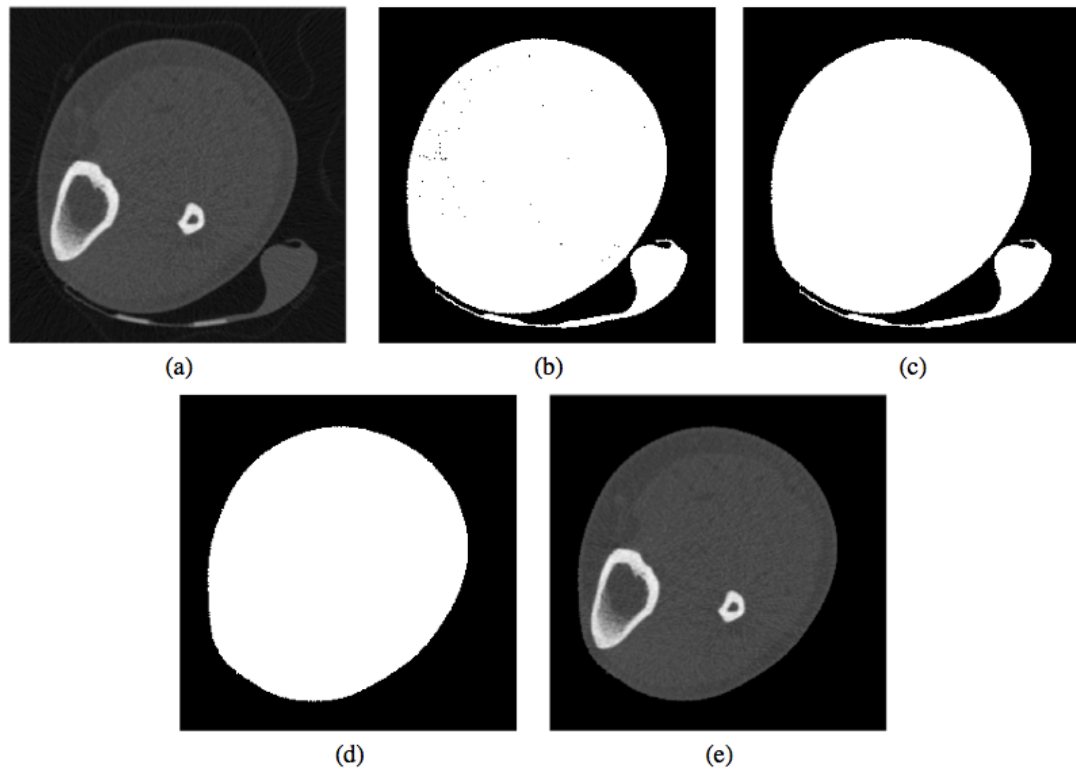

FIGURE 4.4: (a) Image with urine bag and clothing artefact; (b) conversion to binary image; (c) holes filled; (d) extraneous artefacts removed; (e) final image

To achieve this, the image was converted to a binary image, separating out objects within the scan from the surrounding air(Figure 4.4(b)). Any remaining holes within the objects were then filled (Figure 4.4(c)). In order to remove the miscellaneous objects surrounding the leg, any objects that were less than 5000 voxels (2500 mm^2) in size were removed from the image (Figure 4.4(d)). As the size of the leg itself was always greater than 2500 mm^2 in area, it was preserved in the image while the extraneous objects were removed. The binary image could

then be converted back into intensity values, generating an image of the scan containing only the leg cross-section (Figure 4.4(e)). This ultimately allows the image to be analysed further.

It is important to note that several of the images required additional processing, such as that seen in Figure 4.4(a). Since there is a high-density object that is connected flush with the leg cross-section, the miscellaneous object could not be filtered out using the method detailed above. In these cases, the object was manually disconnected from the leg within the CSV file, and was then able to be fully removed with Matlab using the approach discussed above.

4.5   Image Segmentation

4.5.1   Thresholding

Once the leg cross-section was isolated in the image, a distribution of density values within the image could be graphed on a histogram. As seen in Figure 4.5, the frequency of each density value (in mg/cm^3) is represented. A histogram is useful in pQCT image processing as it displays a general separation of different components within the image, particularly between soft tissue and bone.

Histograms are one of the fundamental tools of image processing, presenting image data in a useful, graphical representation. Simple visual inspection of a histogram alone can indicate distinct regions within its corresponding image. Using more complex analysis techniques, it can be used to form the basis of thresholding techniques, which segments the image into useful areas. For pQCT scans of the leg, this ultimately results in the determination of the total area of bone, muscle, and fat within the image.
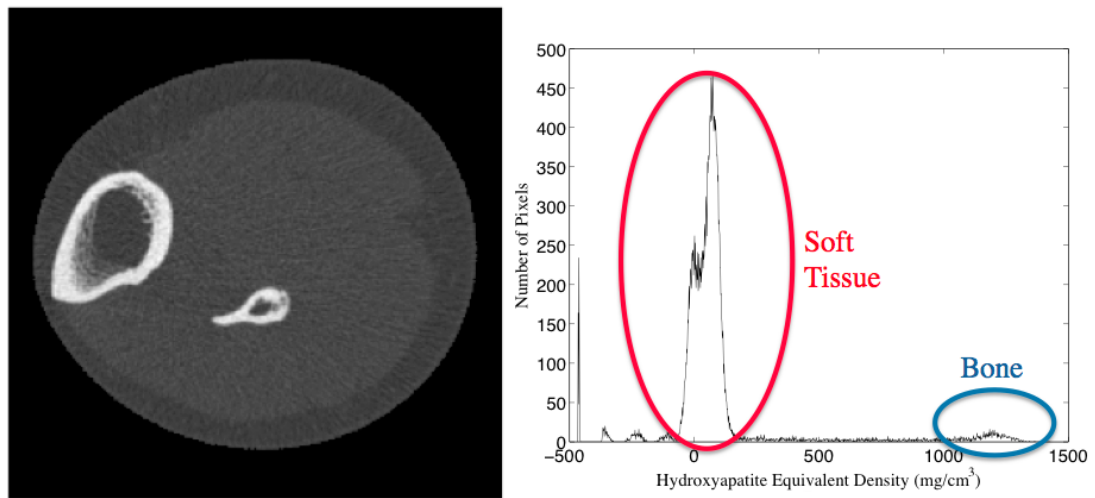
FIGURE 4.5: Image of pQCT scan and its corresponding histogram

Thresholding is a key technique in segmenting the image based on histogram data and interpreting pQCT images. In order to perform this analysis, it is necessary to identify thresholds for each type of tissue. These thresholds are based on density, and separate fat from muscle and from trabecular and cortical bone. Two approaches can be taken in defining density thresholds for the images.

4.5.1.1 Constant Thresholds

In the first approach, constant thresholds can be used to define fat, muscle, bone, and cortical bone. The pQCT manufacturer's software supplies such constant thresholds, where muscle is 34 mg/cm^3, bone is 280 mg/cm^3, and cortical bone is 710 mg/cm^3 (Findlay 2012). However, the density thresholds, especially between fat and muscle, can often vary between patients. Muscle composition has been found to be affected by gender, age, health, and genetics. A reduced CT attenuation in skeletal muscle tissue can be seen in patients with lower muscle quality (Goodpaster et al. 2001), (Goodpaster et al. 2000). Thus, a variable threshold may be better suited in analysing the images.

4.5.1.2 Variable Thresholds

An alternative, more complex, solution would be to define a different threshold for each patient. Using this approach, the bone and cortical bone thresholds will remain constant through all patients using the manufacturer's specifications. However, the muscle threshold will be determined through image processing for each individual patient in order to more accurately segment fat from muscle tissue.

For this study, several different techniques were explored to find the ideal method to segment fat from muscle tissue in each scan. One such solution that was considered involved utilising increased contrast in the images. This allowed the muscle tissue to be more accurately identified from the fat tissue. The primary challenge in this methodology involved ensuring that the contrasting algorithm did not remove critical data. The method was eventually rejected due to its poor success in developing precise thresholds.

The muscle threshold was ultimately determined through segmentation of each image's histogram, such as that seen in Figure 4.5. The first step in this process in generating this histogram involved removal of the large amount of statistical noise present in the original image. This was mitigated through use of a 12x12 gaussian lowpass filter, which was applied to the image using an inbuilt function within Matlab's Image Processing Toolbox. Gaussian filters are frequently applied to medical images in radiology to improve signal to noise ratio before image segmentation (Neri et al. 2007). They work by applying a gaussian function to each individual pixel within an image, with the amount of blurring directly related to the kernel size (Neri et al. 2007). Although the filter degrades the image quality slightly through blurring, it is an effective tool in providing a histogram that can be utilised for calculating thresholds between soft tissue. These thresholds were ultimately implemented on the original image, thus preserving the original data

during tissue quantity calculations. A sample result of this gaussian filter applied
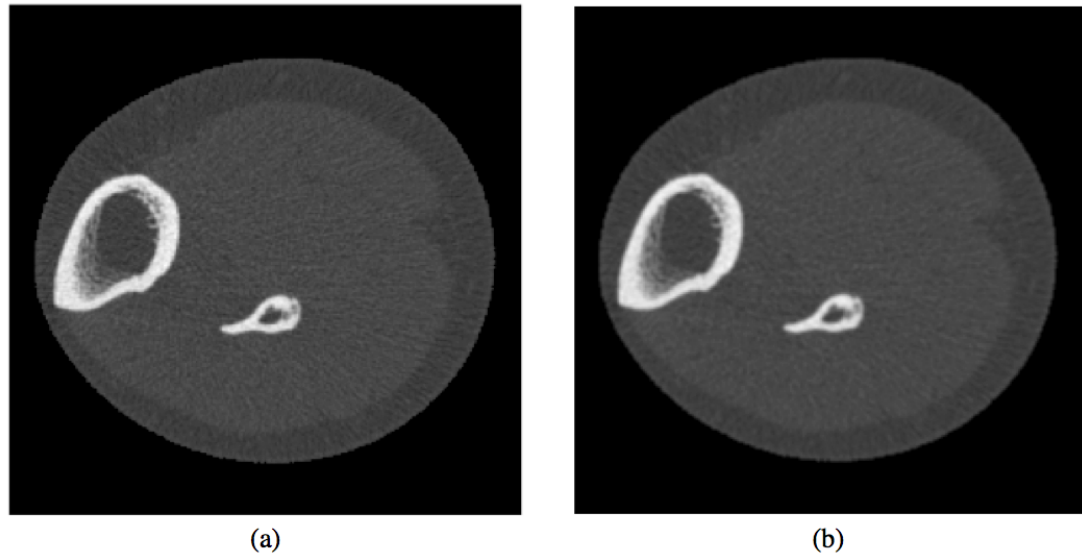to an image can be found in Figure 4.6.

FIGURE 4.6: (a) Original image and (b) gaussian smoothed image

Although the histogram from the gaussian filtered image was improved, some
amount of noise was still present requiring the need for an additional smoothing
filter for the data. This was accomplished using a Savitzky-Golay Finite Impulse
Response (FIR) smoothing filter, completed through an inbuilt function within
Matlab's Signal Processing Toolbox. Savitzky-Golay FIR smoothing filter's are
ideal in smoothing out noise within a signal, while still conserving the general
shape and magnitude of the peaks (Schafer 2011). This function removed any re-
maining noise, allowing the histogram to be more easily analysed (Figure 4.7(b)).

In order to determine the density threshold between fat and bone, the smoothed
histogram was analysed to find where the slope of the curve changed from negative
to positive, indicating the location where the density region of fat changed into
the density region of muscle. This is a novel technique in establishing the density
relationships between fat and muscle. To obtain these data, the first derivative of

the histogram was taken showing the rate of change of densities within the image (Figure 4.7(c)). The first derivative of the histogram is easier to interpret: when the slope of the histogram is positive, the derivative is positive. Conversely, when the slope of the histogram is negative, the derivative is negative. Therefore, to find where the slope of the histogram curve changed from negative to positive, the image processing software needed to find zero-crossings from negative to positive values. Since there were several crossings both at low densities due to noise and at high densities due to bone thresholds, an additional limit needed to be implemented. An assumption was made that the threshold would be greater than the density of fat, so the software searched for the first negative to positive crossing greater than 0 mg/cm^3. In the case of Figure 4.7(c), this first crossing occurs at a density of 2.9 mg/cm^3, thus establishing the threshold between fat and muscle tissue.

Once a threshold had been determined for each image, the threshold was normalised for each patient (given the assumption that an individual's muscle density remained constant over time). Given that each patient received four scans, the calculated thresholds for each subject were averaged. In the final analysis, this constant threshold was then applied to each individual patient.

This method was successful on 70 of the 72 (97%) images that were processed. The two images whose calculated thresholds were rejected were the result of poor image quality due to movement artefact. This was mitigated by basing the threshold on the average of the remaining three images from that patient.

4.5.2 Edge Detection

Using the techniques described above, a general approximation of tissue quantity can be determined based on density thresholds. However, thus far it does not
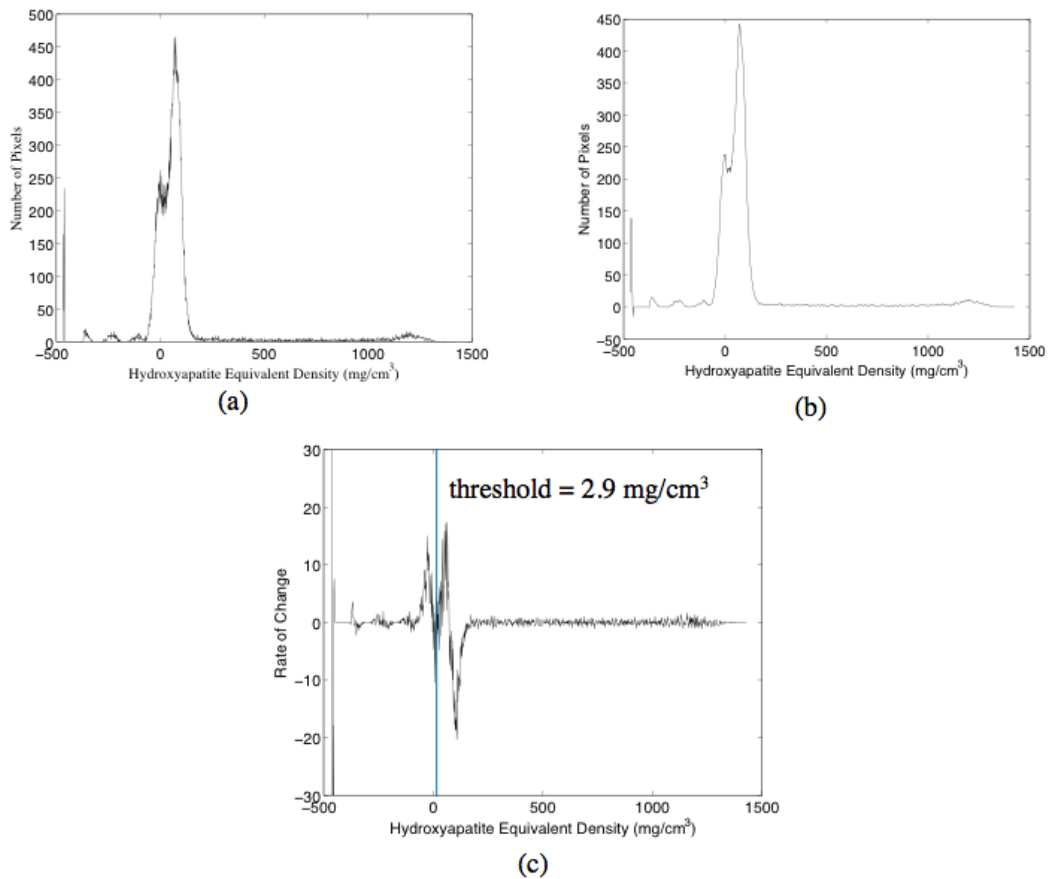
FIGURE 4.7: (a) Histogram with gaussian filter; (b) histogram with Savitzky-Golay FIR filter; (c) first derivative of histogram

account for the area inside the tibia and fibula bones, which is composed of bone marrow. Without removal of the bone marrow from the calculations, this area is the approximate density of muscle and would hence be included as part of the muscle. This area was removed using Sobel edge detection (Dougherty 2009), an inbuilt function within Matlab's Image Processing Toolbox.

First, bone pixels were detected using the thresholds as described in Section 4.5.1. All pixels that were above the bone threshold were then converted into binary (Figure 4.8(b)). Sobel edge detection was then able to generate an outline of the bone (Figure 4.8(c)), which could then be filled (Figure 4.8(d)). The identified

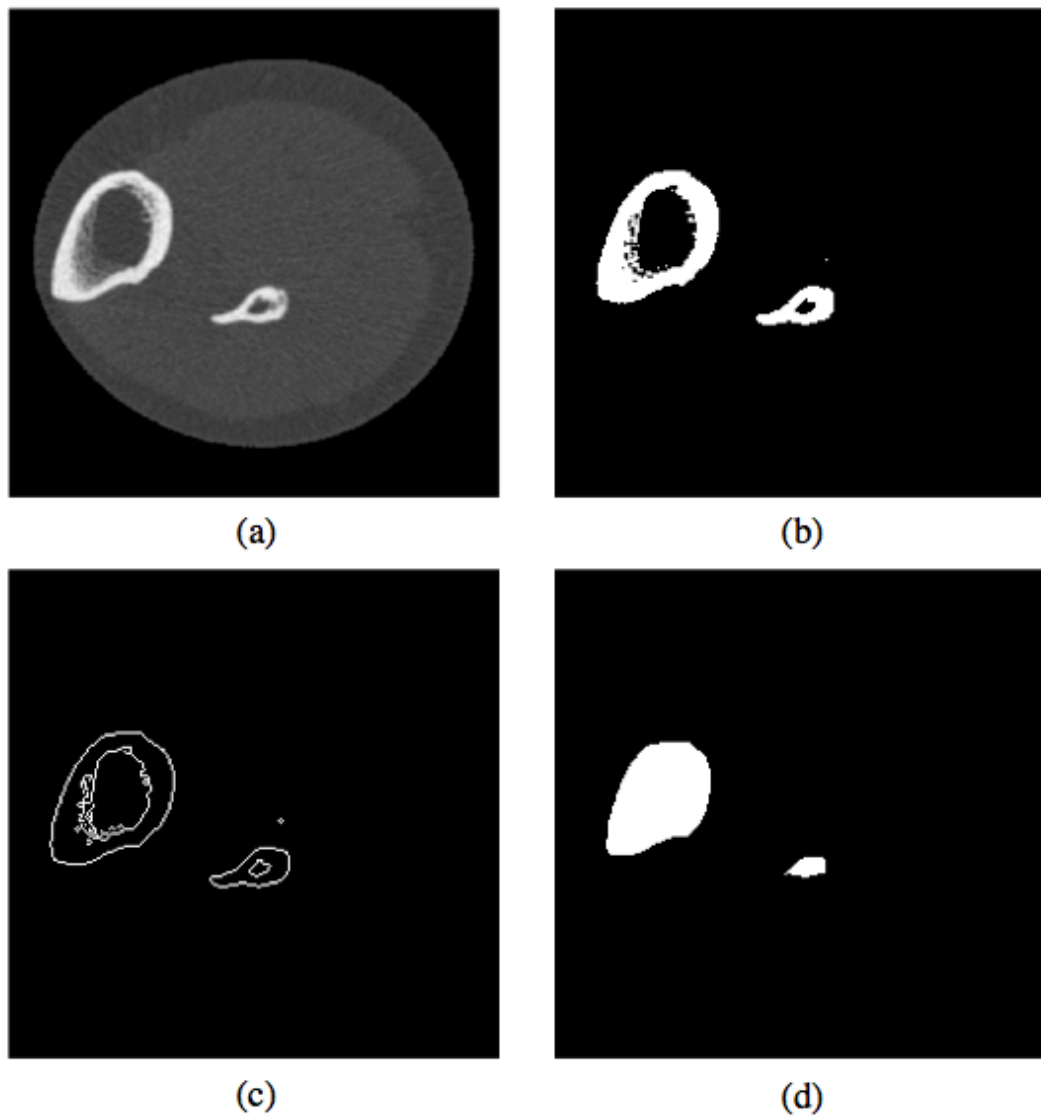pixels were then removed from the soft tissue area calculations.

FIGURE 4.8: (a) Original image; (b) conversion of bone pixels to binary image; (c) Sobel edge detection of bone; (d) fully segmented bone area

4.5.3   Quantisation of Tissue

Once all thresholds are determined, the number of voxels from within each threshold could be calculated. Knowing that each voxel has an edge size of 0.5 mm,

the cross-sectional area of fat, muscle, bone, and cortical bone within the scan was determined. This can be visualised using colour representation as seen in Figure 4.9. In this image, fat is represented as yellow, muscle is represented as red, trabecular bone is represented as grey, cortical bone is represented as white, bone marrow is represented as blue.
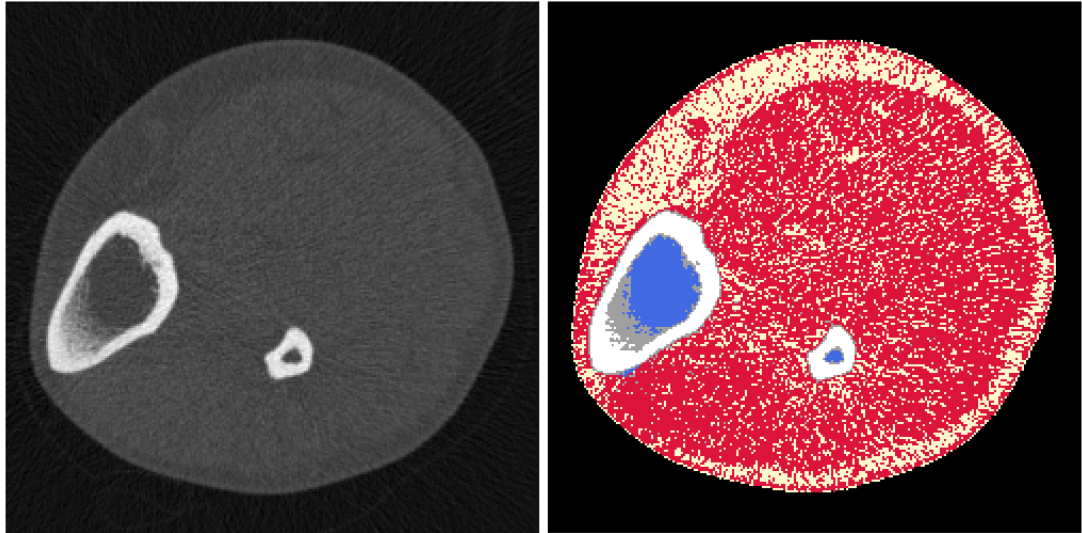

FIGURE 4.9: Image segmentation using thresholds

The geometric parameters that were isolated from each image included:

- Fat cross-sectional area (CSA_{fat}): cross-sectional area of fat tissue (mm^2)

- Fraction of fat (f_{fat}): fraction of the leg cross-section that is composed of fat

- Muscle cross-sectional area (CSA_{muscle}): cross-sectional area of muscle tissue (mm^2)

- Fraction of muscle (f_{muscle}): fraction of the leg cross-section that is composed of muscle

- Bone cross-sectional area (CSA_{bone}): cross-sectional area of bone, including both trabecular bone and cortical bone, not including inner cavity (mm^2)

- Fraction of bone (f_{bone}): fraction of the leg cross-section that is composed of bone, including both trabecular bone and cortical, not including the inner cavity

- Cortical bone cross-sectional area ($CSA_{cortical}$): cross-sectional area of cortical bone (mm^2)

- Fraction of cortical bone ($f_{cortical}$): fraction of the leg cross-section that is composed of cortical bone

- Bone marrow cross-sectional area (CSA_{marrow}): cross-sectional area of the inner cavity of tibia and fibula (mm^2)

- Fraction of bone marrow (f_{marrow}): fraction of the leg cross-section that is composed of bone marrow

Representative data corresponding to Figure 4.9 can be seen in Table 4.2

TABLE 4.2 Sample data

Muscle Threshold	5 mg/cm^3
Bone Threshold	280 mg/cm^3
Cortical Bone Threshold	710 mg/cm^3
CSA_{fat}	3227 mm^2
f_{fat}	19.4%
CSA_{muscle}	11085.5 mm^2
f_{muscle}	66.5%
CSA_{bone}	1053.5 mm^2
f_{bone}	6.3%
$CSA_{cortical}$	758 mm^2
$f_{cortical}$	4.5%
CSA_{marrow}	538 mm^2
f_{marrow}	3.2%

The data collected from each individual scan could then be used to calculate the percent change in CSA, ΔCSA, of each tissue between scan times for each subject. The changes for each tissue were all calculated with respect to the baseline scan. This included:

- Change in CSA_{fat} ($\Delta CSA_{fat,T2}$, $\Delta CSA_{fat,T3}$, and $\Delta CSA_{fat,T4}$): percent change in fat CSA between the baseline scan and T2, T3, and T4, respectively

- Change in CSA_{muscle} ($\Delta CSA_{muscle,T2}$, $\Delta CSA_{muscle,T3}$, and $\Delta CSA_{muscle,T4}$): percent change in muscle CSA between the baseline scan and T2, T3, and T4, respectively

- Change in CSA_{bone} ($\Delta CSA_{bone,T2}$, $\Delta CSA_{bone,T3}$, and $\Delta CSA_{bone,T4}$): percent change in bone CSA between the baseline scan and T2, T3, and T4, respectively

- Change in $CSA_{cortical}$ ($\Delta CSA_{cortical,T2}$, $\Delta CSA_{cortical,T3}$, and $\Delta CSA_{cortical,T4}$): percent change in cortical bone CSA between the baseline scan and T2, T3, and T4, respectively

Each of these data were acquired using a Graphical User Interface (GUI) that was developed within the Matlab environment for this project. Data could be output for individual files or for a range of files, using either variable or constant thresholds. Examples of this functionality can be seen in Appendix A.

4.5.4 Limitations of Image Segmentation

Despite the benefits of using this novel thresholding technique, some limitations existed. The first was the inability of the presented technique to account for skin

within the leg cross-sectional image. As seen in Figure 4.9, the outer pixels of the leg were distinguished as muscle, though the more likely explanation is that this region was skin. In other words, this technique identified skin as muscle due to the similarities in their densities. However, due to the inability of pQCT to provide accurate quantisation of lipid content within the muscle (Schick et al. 2002), the skin was considered to be a negligible error in comparison and thus was unaccounted for in the analysis.

An additional limitation of this technique lies within the Sobel edge detection in identifying bone marrow. Because of the inherent properties of this method, some of the images show several pixels of bone marrow lying outside of the cortical bone area, as seen in Figure 4.9. However, this effect was also minor and did not significantly affect the output of the results.

4.6 Trabecular Bone Changes in the Proximal Epiphysis

To provide additional data for this study, completed datasets of the changes in BMD in the trabecular bone of the proximal tibial epiphysis were obtained from Dr. Sylvie Coupaud. These data were collected from pQCT scans at the 96% distal tibia, and were gathered for 16 of the 18 subjects used in this study.

Chapter 5

Results

5.1 Comparison of Variable & Constant Thresholds

5.1.1 Results

Data from eighteen subjects were taken during the course of this study. For each scan, the cross-sectional area for each type of tissue was obtained using both constant thresholds and variable thresholds. These data were then used to calculate the percent change in CSA over time for each individual for both thresholding techniques. These results can be found in Table 5.1.

The data obtained through the use of constant thresholds is defined in Section 4.5.1.1. In this case, the threshold for muscle was 34 mg/cm^3, the threshold for bone was 280 mg/cm^3, and the threshold for cortical bone was 710 mg/cm^3 (Findlay 2012) for all patients.

TABLE 5.1 Changes in soft tissue and bone using constant and variable thresholds ($n = 18$)

Tissue	ΔCSA_{T2}		ΔCSA_{T3}		ΔCSA_{T4}	
	Constant	Variable	Constant	Variable	Constant	Variable
Fat	$12.1\% \pm 22.9$	$12.1\% \pm 23.8$	$23.1\% \pm 29.3$	$25.9\% \pm 31.9$	$34.6\% \pm 37.7$	$39.2\% \pm 42.4$
Muscle	$-1.4\% \pm 16.6$	$-0.1\% \pm 16.3$	$-6.2\% \pm 15.4$	$-4.2\% \pm 15.4$	$-6.8\% \pm 16.9$	$-4.4\% \pm 17.3$
Bone	$-0.5\% \pm 0.9$		$-0.7\% \pm 1.2$		$-1.6\% \pm 2.5$	
Cortical Bone	$-0.7\% \pm 0.8$		$-1.4\% \pm 1.5$		$-2.5\% \pm 2.3$	

Results expressed as mean ± standard deviation

5.1.2 Verification of Software

To ensure that variable thresholding between fat and muscle tissue was a viable technique, the results were compared against the use of constant thresholds.

Since the thresholds for bone/cortical bone were defined as constants in both cases, there was no difference in the percent change of bone. Thus, statistical

analysis was performed on data collected of the percent change in muscle (including baseline to T2, baseline to T3, and baseline to T4). The statistical method used was originally presented by Bland & Altman (1986) for use in evaluating the agreement between two clinical measurement techniques, and is thus an appropriate approach to assessing the agreement between the two thresholding approaches for pQCT scans. Figure 5.1 shows a plot of the mean of the two techniques vs. the difference between the two techniques, which aids in evaluating the relationship between fixed thresholds and variable thresholds.
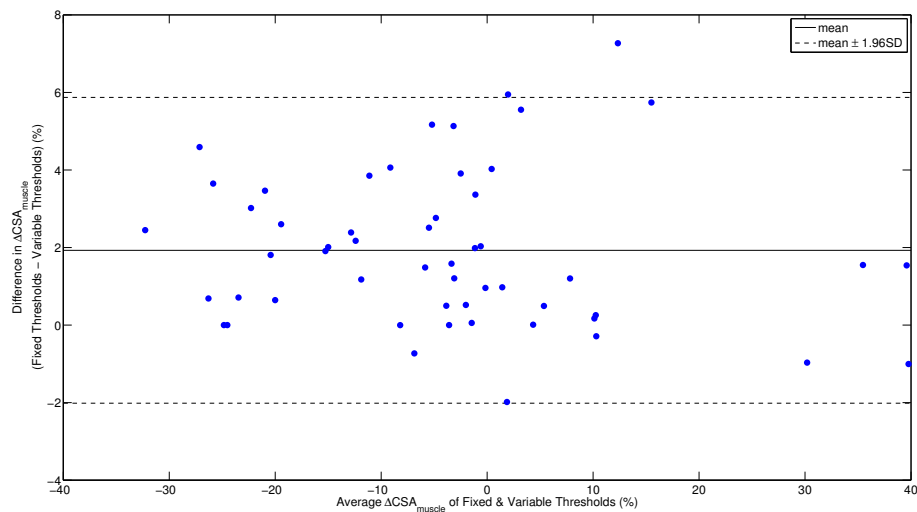
FIGURE 5.1: Mean vs. difference of the percent change in muscle CSA data

For the ΔCSA data, the mean difference between the two techniques was 1.9% with a standard deviation (SD) of 2.0%. Using a gaussian normal distribution for the differences, 95% of the differences should lie between the limits described by the mean $\pm$ 1.96SD. For this data, the range of differences was -2.0% to 5.9%.

For further analysis into the differences between constant and variable thresholding techniques, a paired sample t-test was performed. Under an alpha significance

level of 0.05, there was a rejection of the null hypothesis ($p = 1.6 \times 10^{-8}$), indicating that there were significant differences in the results of the two methodologies.

5.2   Individual Subject Examples

During data collection using the variable threshold methodology, trends in tissue changes were found to vary between patients. For the majority of images, tissue changes over time indicated a typical trend, where the quantity of both muscle and bone decreased while the quantity of fat increased following SCI. However, other subjects showed atypical results, either showing no apparent changes in tissue quantity, or displaying trends that were converse to what was expected, especially with respect to muscle cross-sectional area. Sample images and data for three individuals are presented in this section. These data sets are representative of both typical results and abnormal results.

5.2.1 Typical Changes in Tissue

As presented in Chapter 2, past studies have indicated that typical changes in tissue following SCI are expected to be manifested as an increase in fat, a decrease in muscle, and a decrease in bone. This subject presented with typical results that illustrate this trend.
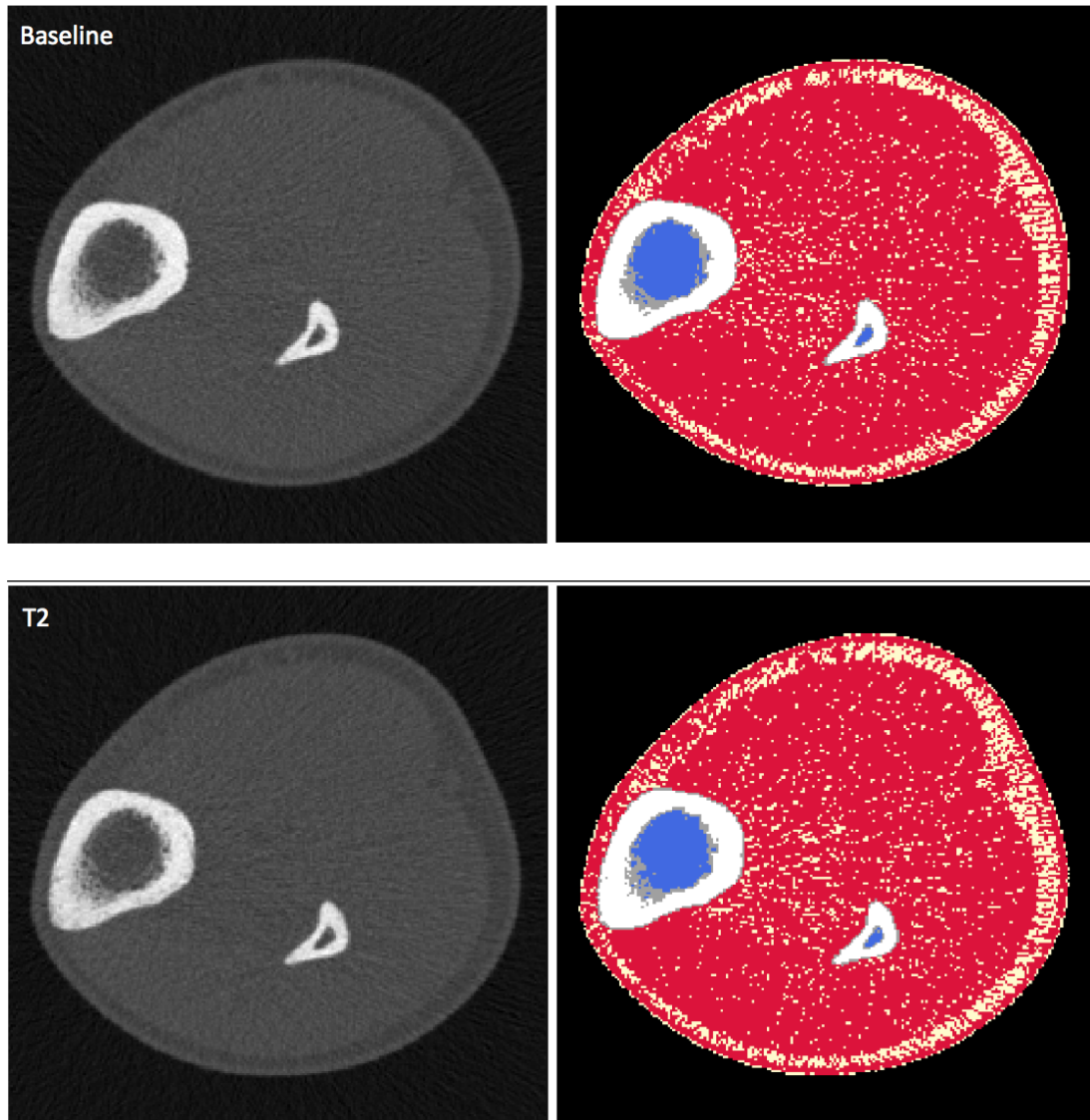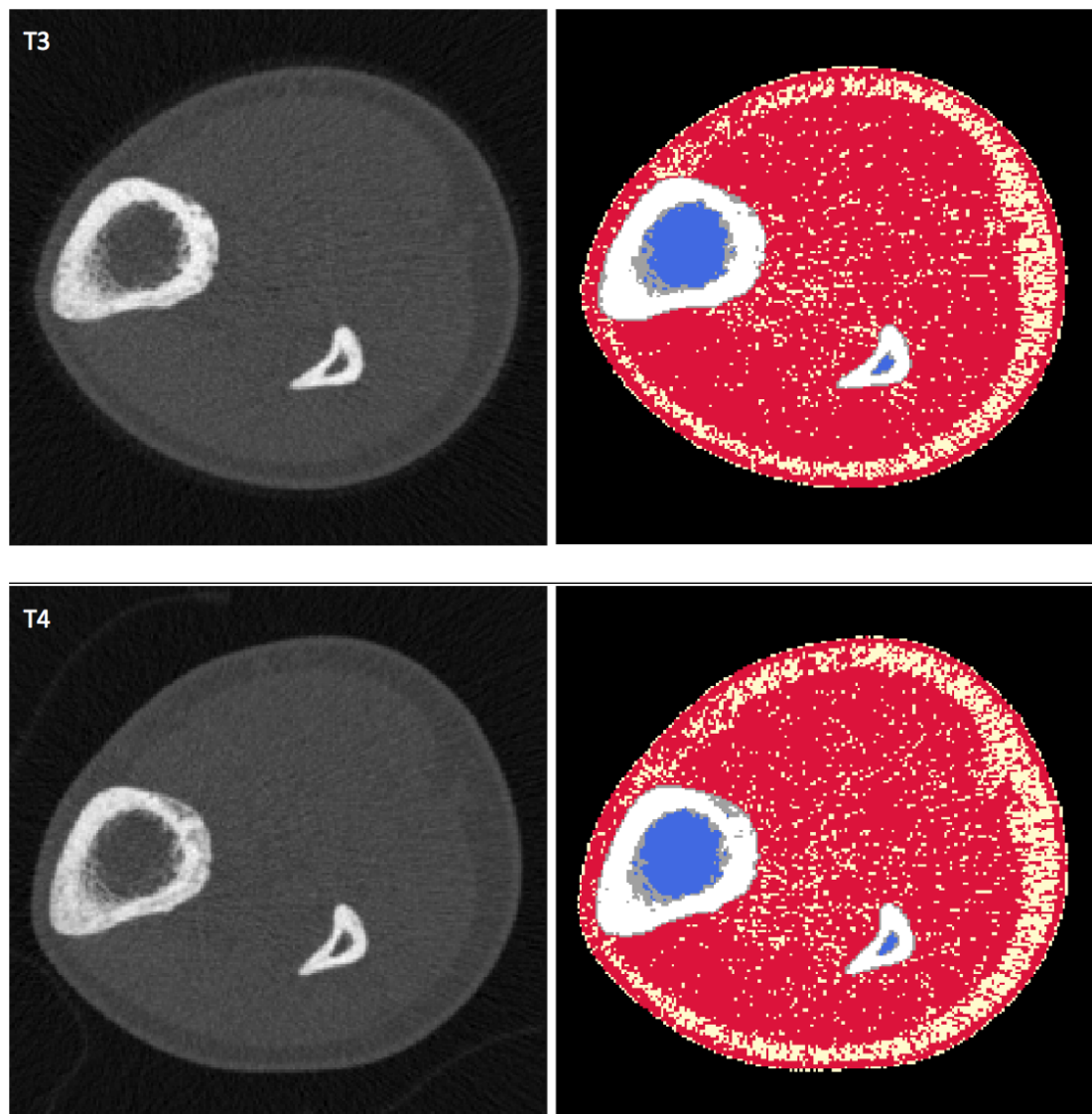
FIGURE 5.2: pQCT scans indicating typical changes in tissue following SCI

The segmented images in Figure 5.2 show visible changes over time, especially with respect to the cross-sectional area of muscle. This change can be further visualised graphically in Figure 5.3. Fat area trended upwards as time progressed. After 12 months, the increase in fat cross-sectional area was 18.0%. Muscle area decreased at each successive scan, resulting in a 24.8% decrease in muscle cross-sectional area after 12 months. Likewise, the cortical bone area decreased as well,

ending with 5.6% decrease in cortical bone cross-sectional area after 12 months.
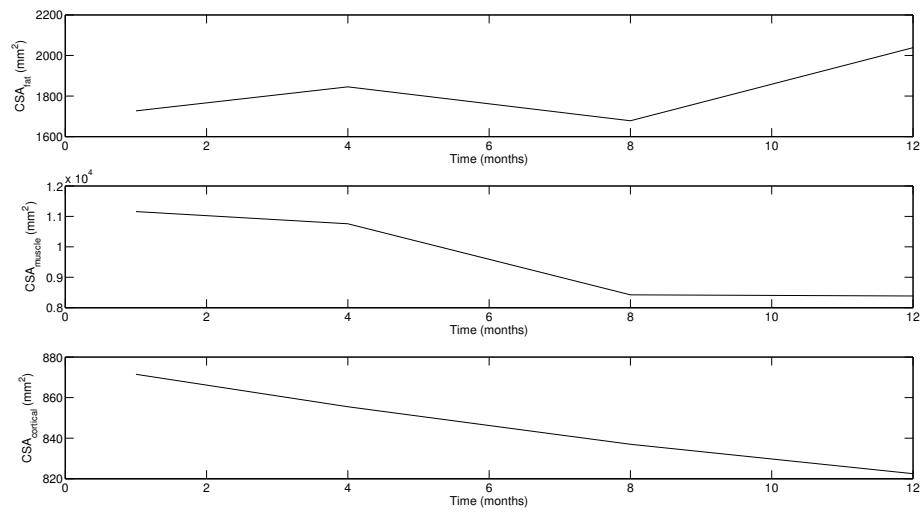
FIGURE 5.3: Plot of typical changes in tissue following SCI

In order to visualise the relationships between muscle and bone in the pQCT scans, the cross-sectional area of muscle vs. bone was plotted in Figure 5.4. In this example, a linear relationship can be found: as the time post-SCI increased, both the muscle cross-sectional area and the cortical bone cross-sectional area decreased. According to previous studies, this data follows the anticipated changes in musculoskeletal tissues following lower limb paralysis.
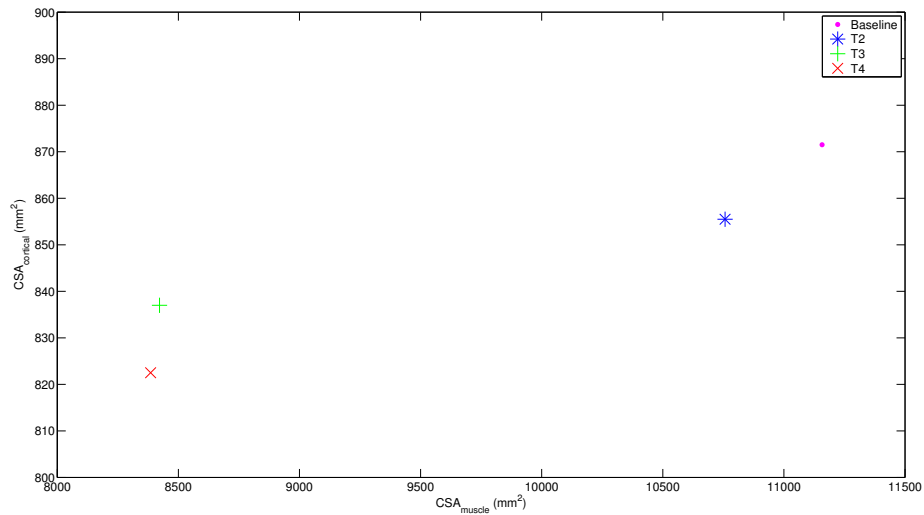
FIGURE 5.4: Muscle-bone relationships with a typical trend following SCI

5.2.2 No Apparent Changes in Tissue

Several subjects studied showed no significant changes in tissue following SCI. Figure 5.5 shows an example of this scenario.

The segmented images in Figure 5.5 show no visible changes over time. A more detailed view of tissue cross-sectional area changes can be seen in Figure 5.9. As expected, the fat area trended upwards as time progressed. After 12 months, the increase in fat cross-sectional area was 42.6%. In addition, the cortical bone was found to decrease as anticipated, with a 3.4% decrease in cortical bone cross-sectional area after 12 months. However, the muscle area showed no significant change over the 12 month time period. At 4 months post-SCI, the muscle quantity had decreased from the baseline scan. At 8 months post-SCI, however, the muscle quantity had increased above the baseline scan. Ultimately, at 12 months post-SCI, the decrease in muscle cross-sectional area was only 5.1%.
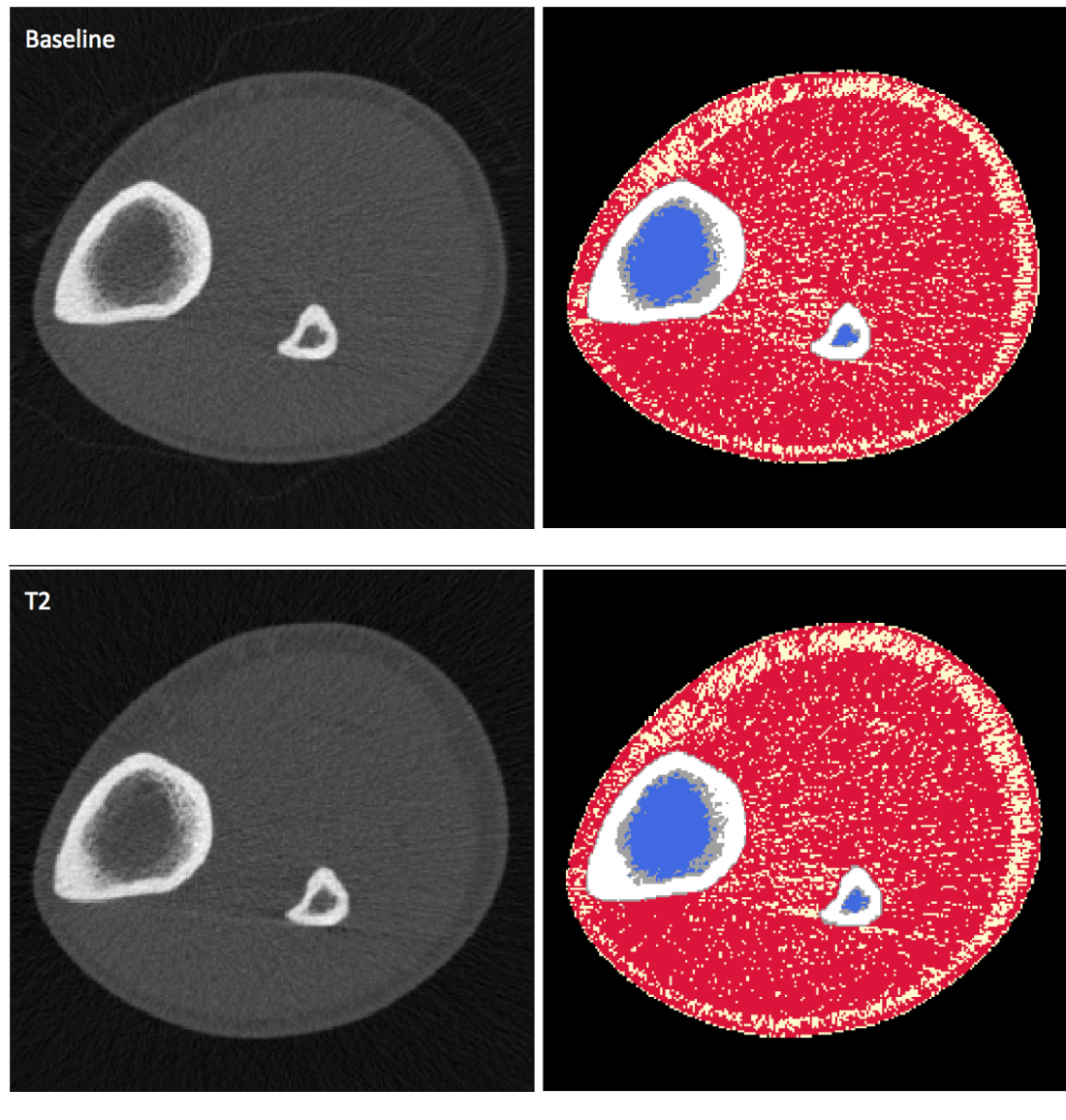
In order to visualise the relationships between muscle and bone in the pQCT scans, the cross-sectional area of muscle vs. bone was plotted in Figure 5.7. In this example, no apparent trend in data can be seen.
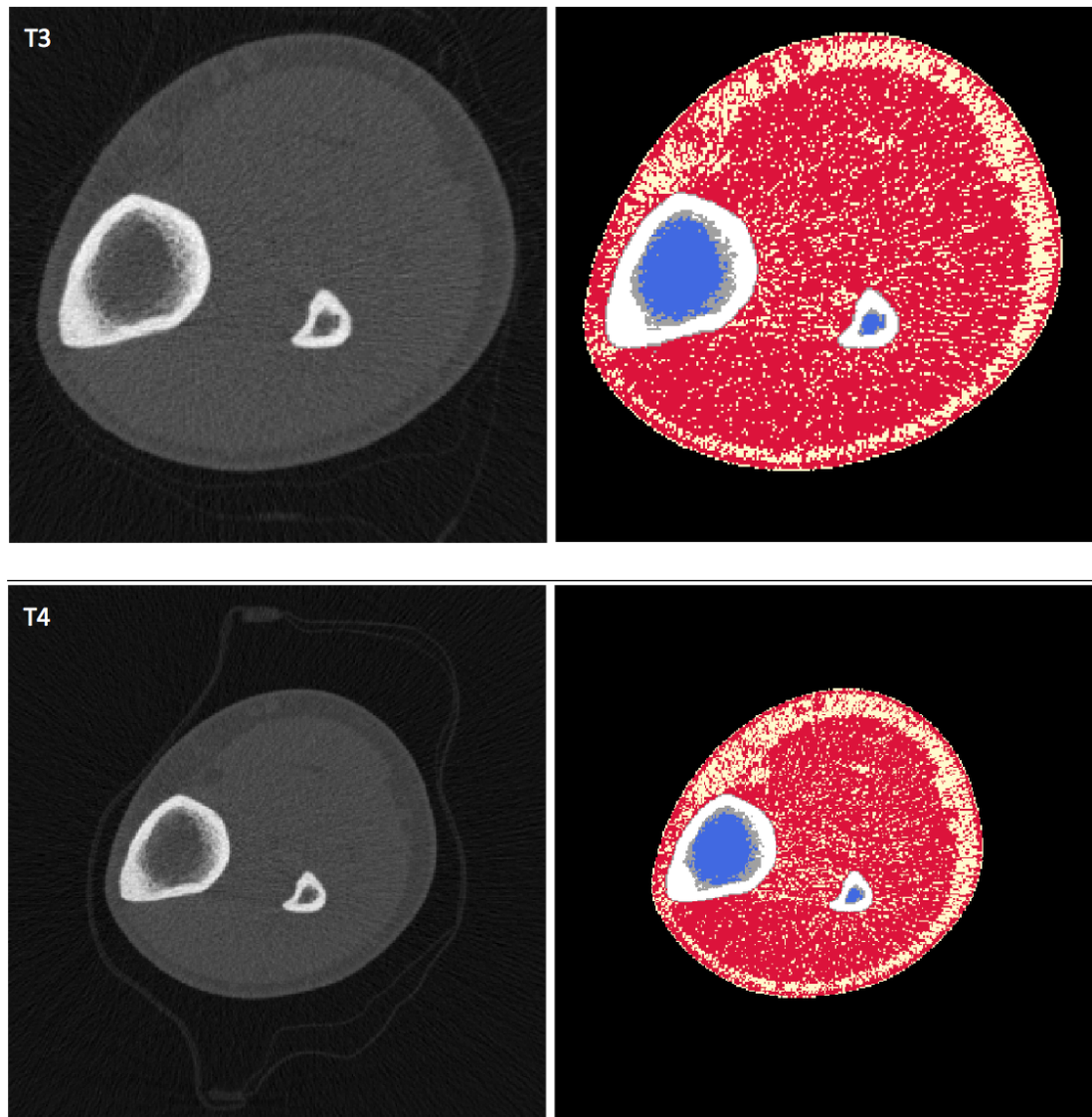
FIGURE 5.5: pQCT scans indicating no apparent significant changes in tissue following SCI (note: images are not to the same scale)
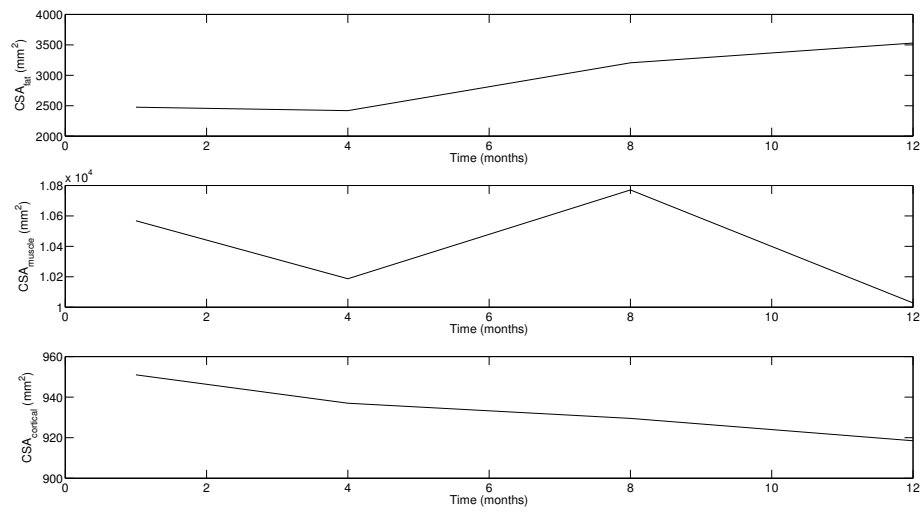
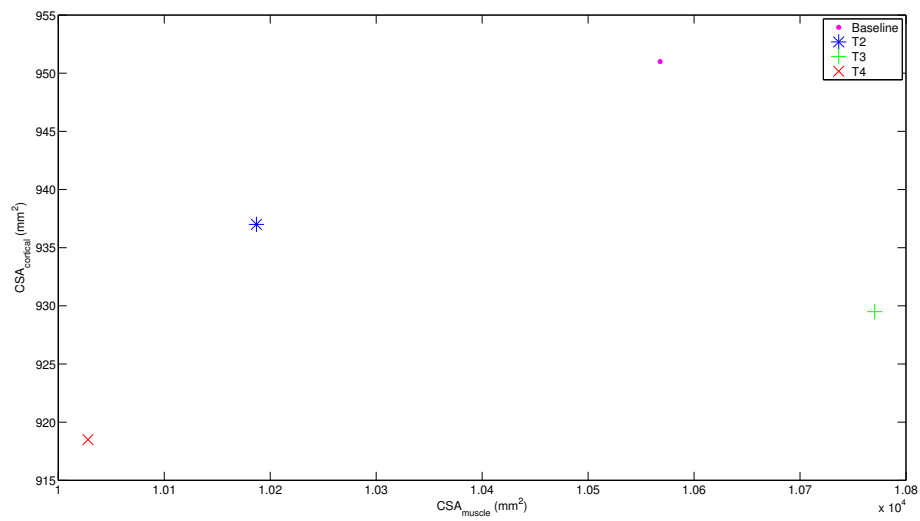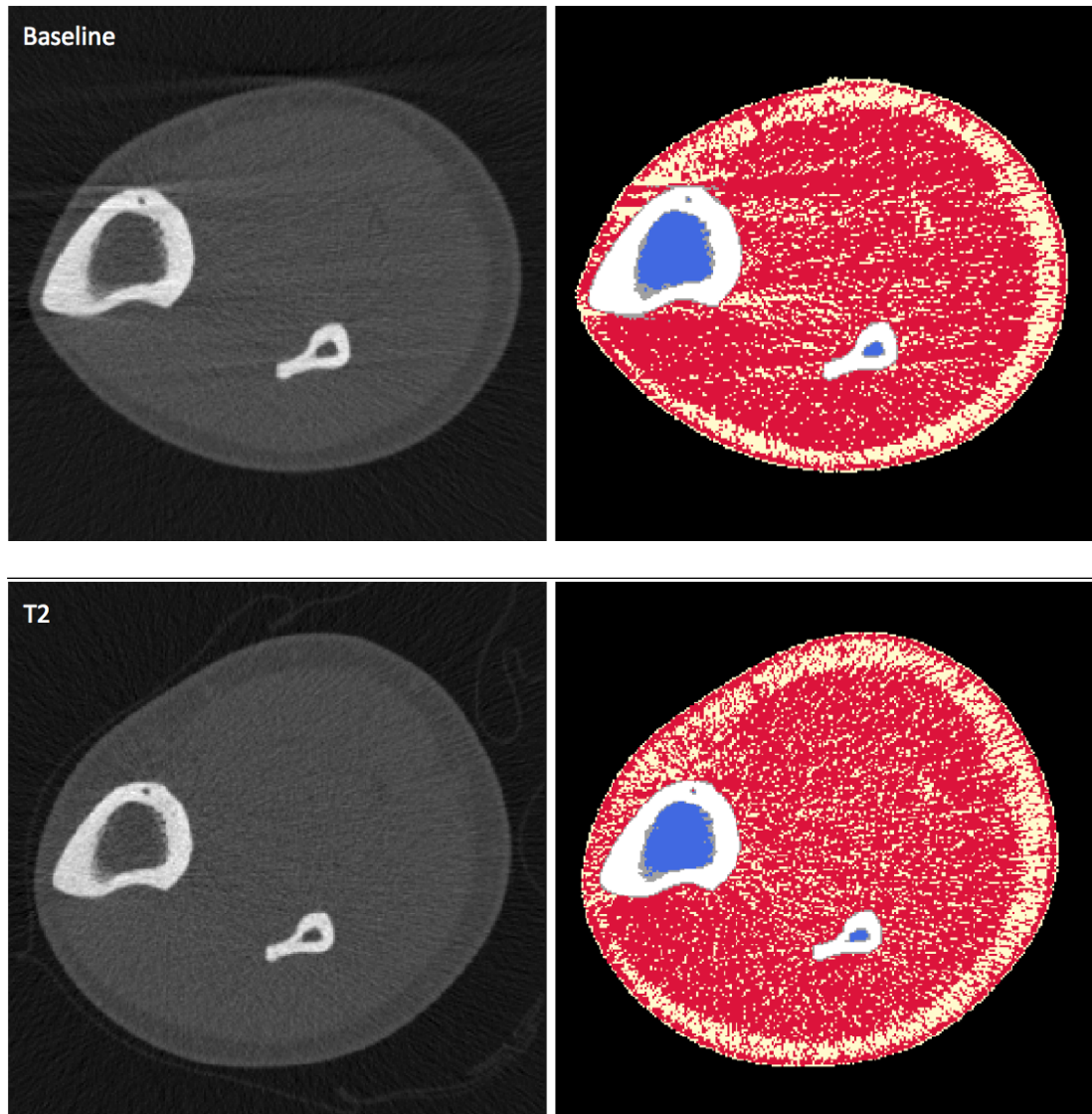FIGURE 5.6: Plot of no apparent significant change in tissue following SCI

FIGURE 5.7: Muscle-bone relationships with no apparent trend following SCI

5.2.3 Unexpected Changes in Tissue

Several subjects studied showed unexpected and atypical changes in tissue following SCI. Figure 5.5 shows an example of this scenario.

Although the segmented images in Figure 5.8 show little visible change over time, a more detailed view of tissue cross-sectional area changes can be seen in Figure 5.9. The trend in fat cross-sectional area was expected: after 12 months
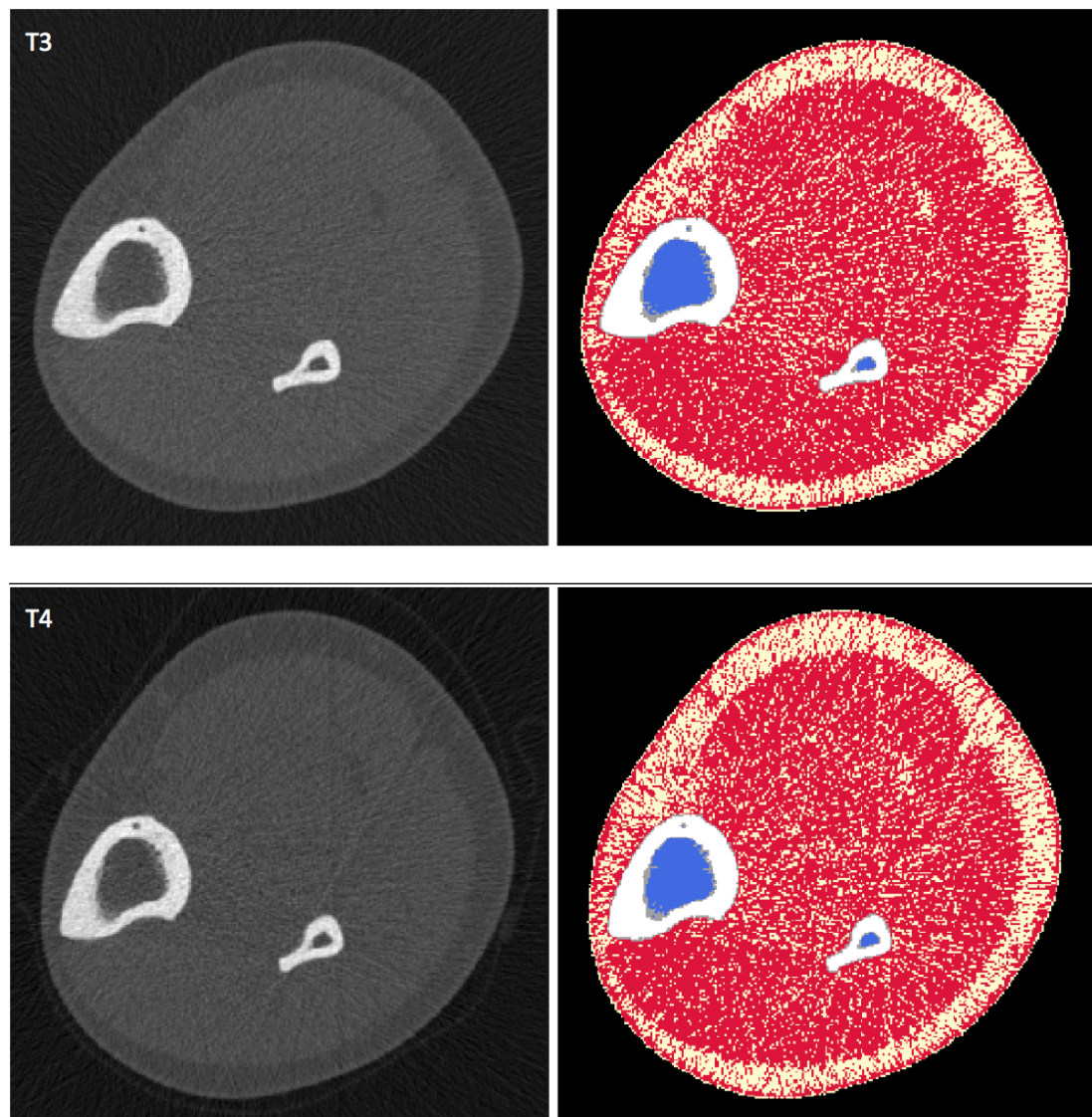
FIGURE 5.8: pQCT scan showing unexpected changes in tissue following SCI

post-SCI, the quantity of fat had increased by 84.6%. The trend in cortical bone cross-sectional area was also typical, showing a downward trend over time, and ultimately resulting in a 1.5% loss in cortical bone after 12 months. However, the cross-sectional area of muscle trended upwards as time progressed, which was unexpected following paralysis. When compared to the baseline scan, the muscle cross-sectional area had increased 40.4% at the 12 month scan.
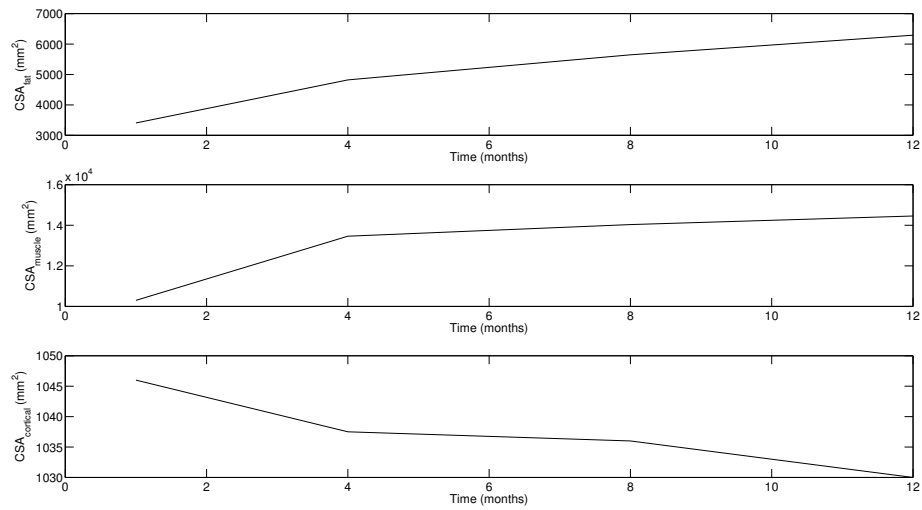
FIGURE 5.9: Plot of unexpected changes in tissue following SCI

In order to visualise the relationships between muscle and bone in the pQCT scans, the cross-sectional area of muscle vs. bone was plotted in Figure 5.10. In this example, a trend can be seen between the two variables: as the time post-SCI increases, the muscle cross-sectional area increased and the cortical bone cross-sectional area decreased. However, this data is not consistent with previous studies on SCI patients.
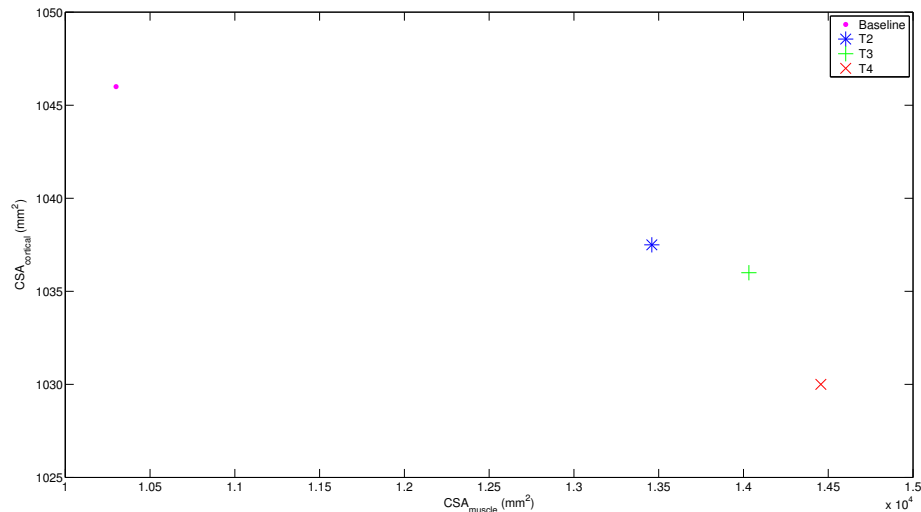
FIGURE 5.10: Muscle-bone relationships with an unexpected trend following SCI

5.3 Predictive Capacity of pQCT Scans

The ultimate objective of this study was to determine if there is a predictive capacity in early pQCT scans following SCI. Ideally, an interrelationship between early muscle loss following paralysis and future bone loss through the use of pQCT scans alone could be established. To characterise the changes in muscle and changes in bone, two relationships were identified. The first established a relationship between muscle loss and cortical bone loss in the diaphysis of the tibia. As discussed in Chapter 2, in the bone shaft, the cortical bone cross-sectional area should have a significant change following lower limb paralysis. Conversely, the density of trabecular bone in the epiphyses should see the most significant changes over time. Thus, the second relationship in this study was a comparison of muscle loss and trabecular bone loss in the proximal tibia.

5.3.1 Comparison of Muscle Changes to Cortical Bone Changes in the Diaphysis

In order to test the capacity of early pQCT scans to predict future bone loss in a patient, the percent change in muscle between the baseline scan at 4 months post-injury was compared against the percent change in cortical bone at 12 months post-injury at the 66% distal tibia. Since several outliers from within the data skewed the results, they were first identified through the use of box plots (Figure 5.11 and Figure 5.12) and then removed from the data set.
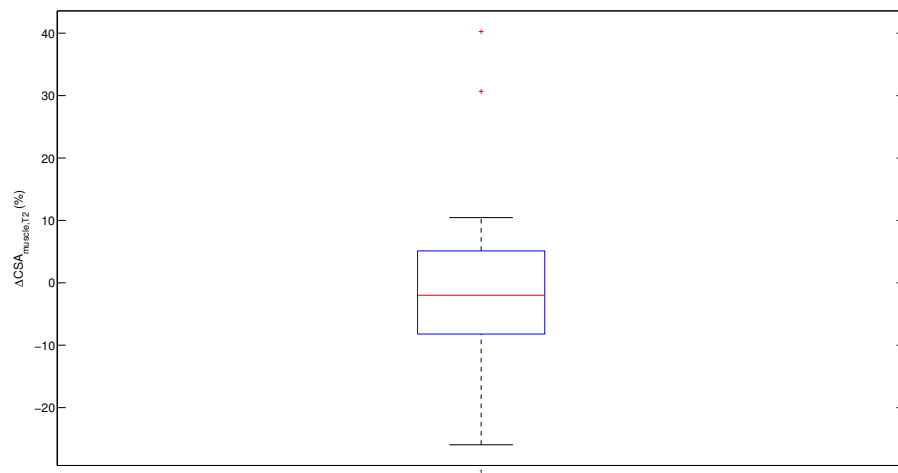

FIGURE 5.11: Box plot of change in muscle CSA between baseline and T2

Both of the outliers discovered for changes in muscle CSA between baseline and T2 were correlated with patients who had worn pressure stockings during the baseline scan. As a result, the muscle CSA was likely reduced at the baseline scan due to the external pressure on the leg, skewing the results. Thus, both of these data points were removed.
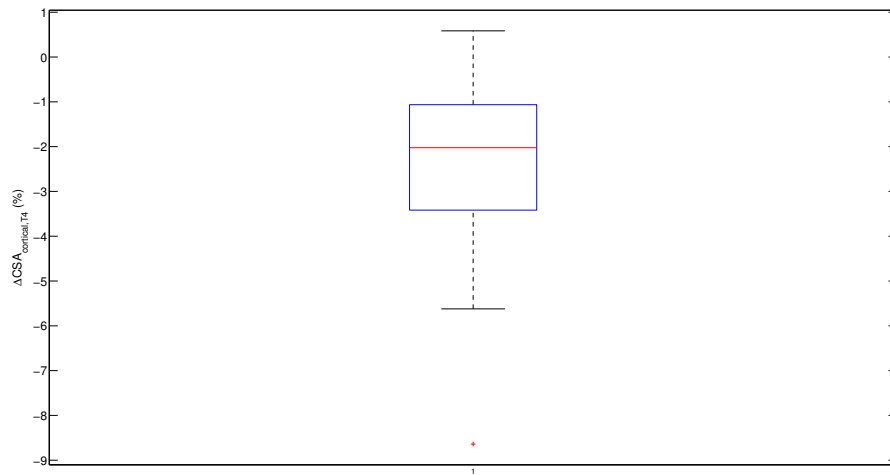
FIGURE 5.12: Box plot of change in cortical bone CSA between baseline and
T4

Once the three outliers were removed from the data set, the remaining data ($n =$
15) was plotted using simple linear regression. Figure 5.13 shows the relationship
between the change in muscle CSA between the baseline scan and T2 scan vs.
the change in cortical bone CSA between the baseline scan and T4 scan. The
Pearson's correlation coefficient (r) for this data was found to be 0.27.

To test the significance of the correlation, a two-tailed test ($n = 15$) was performed
with a significance level of 0.05. For this test, the null hypothesis was defined as
$r \leq 0$ and the alternative hypothesis was defined as $r > 0$. The resultant critical
value (p) for these parameters was 0.51, indicating that the correlation between
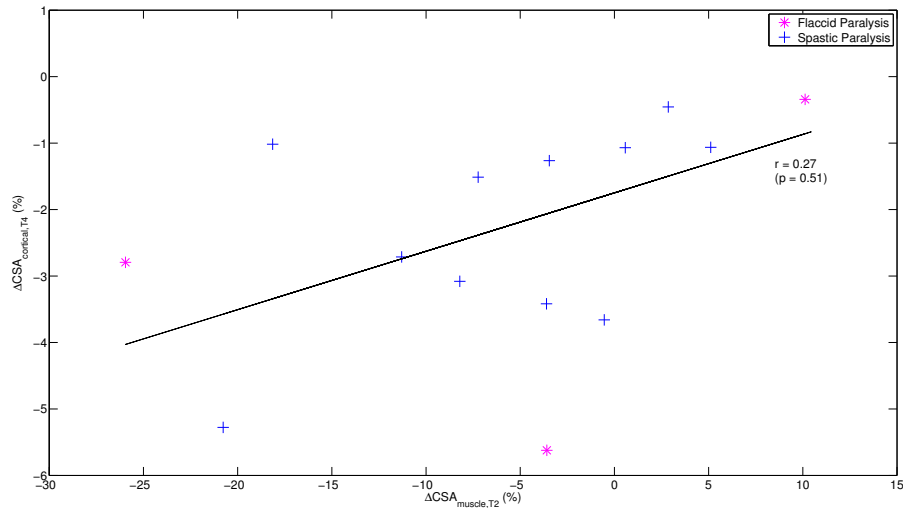muscle loss and cortical bone loss was not statistically significant.

Figure 5.13: Comparison of change in muscle CSA vs. change in cortical bone CSA ($n = 15$)

5.3.2 Comparison of Muscle Changes to Trabecular Bone Changes in the Proximal Epiphysis

As no significant relationship was detected between muscle loss and cortical bone loss, the separate data set of BMD changes in the proximal epiphysis of the tibia was studied. For this analysis, the change in trabecular bone density after 12 months at this scan location was compared to the change in muscle CSA between the baseline scan and T2 scan at the 66% distal tibia.

As in Section 5.3.1, the outliers were first identified and removed from the data set. The muscle outliers were identified through Figure 5.11. No further outliers were identified within the change in trabecular bone data set, as seen in Figure 5.14.

A linear regression could then be performed through the change in muscle CSA between the baseline scan and T2 scan vs. the change in trabecular bone density
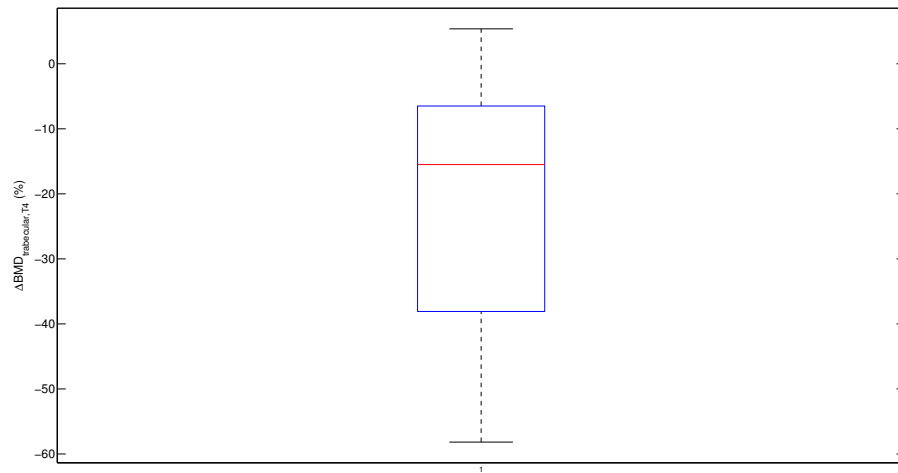
FIGURE 5.14: Box plot of change in trabecular bone density at the proximal tibia between baseline and T4 ($n = 14$)

between the baseline scan and T4 scan. In this case, the Pearson's correlation coefficient was found to be 0.02.

To test the significance of the correlation, a two-tailed test ($n = 14$) was performed with a significance level of 0.05. For this test, the null hypothesis was defined as $r \leq 0$ and the alternative hypothesis was defined as $r > 0$. The resultant critical value for these parameters is 0.53, indicating that the correlation between muscle loss and trabecular bone loss at the proximal epiphysis was not statistically significant.
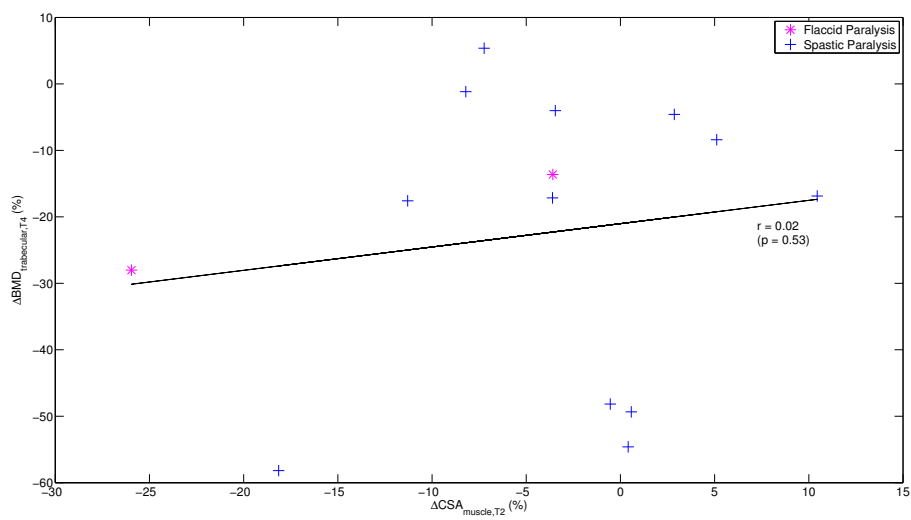
FIGURE 5.15: Comparison of change in muscle CSA vs. change in trabecular bone density at the proximal tibia

Chapter 6

Discussion

Verification of the automatic threshold technique was performed using the statistical method defined by Bland & Altman (1986). From these data (seen in Figure 5.1), it can be surmised that a constant threshold typically showed a greater change in muscle CSA than variable thresholding by an average of 1.9%.

Using variable thresholds, the calculated threshold was lower than 34 mg/cm^3 for most subjects (15 of 18). As a result, variable thresholds identified more of the voxels within the scan as muscle tissue. As mentioned in Section 4.5.1.1, the density of muscle may be affected by muscle quality. Most notably, an increased intercellular lipid content within the muscle results in a lower density value in pQCT scans (Goodpaster et al. 2000). By using variable thresholds that were averaged across each subject's scan, changes in muscle quality were better accounted for. In contrast, a constant universal threshold identified a higher portion of the voxels as fat. However, some of these voxels were likely a reduced quality muscular tissue which had developed over time. Therefore, segmentation using constant thresholding displayed a higher ΔCSA_{muscle}. Due to this effect, variable thresholding is more suitable for distinguishing muscle tissue from fat tissue.

The means of the raw data found in Table 5.1 (variable thresholding) show the expected trends in changes of soft tissue and bone cross-sectional areas. As the time post-SCI increases, the quantity of fat increases up to approximately 39.2% 12 months post-SCI, while the quantities of muscle and cortical bone decrease up to -4.4% and -2.5% 12 months post-SCI, respectively. Increases in subcutaneous fat are visible in the pQCT scans of most subjects, manifested through an increase in thickness of fat surrounding the muscle. This effect can be seen all three subjects presented in Chapter 5.

In addition, voxels segmented as fat tissue can be seen scattered within the muscle itself. Some of the individual voxels seen in the images can be attributed

to additional lower-density muscle that the variable thresholding was unable to account for. However, intramuscular fat was also visible on several scans. This effect was manifested as small clusters of fat, most often seen in images taken at T3 or T4 (this effect can be seen clearly within the T4 scan of Figure 5.5).

The general trends seen in Table 5.1 are consistent with past studies examining changes in tissue following SCI. In the study by Castro et al. (1999), muscle CSA had decreased by 24% in the *m.* gastrocnemius and by 12% in the *m.* soleus after 18 weeks. This time period correlates well between the baseline and T2 scans of this study, which shows and change in muscle CSA of $-0.1\% \pm 16.3$ (using variable thresholds). Although pQCT cannot distinguish between the two muscle groups, it is still evident that the changes in muscle quantity were much less pronounced in this study than that performed by Castro et al. (1999). This may be due to the timing of the baseline scans. Since muscle atrophy occurs so rapidly following immobilisation (up to 45% within the first month (Castro et al. 1999)), any differences in the timing of the baseline scan would be significant. In addition, the length of time between scans was two weeks longer in the study by Castro et al. (1999), which may have shown a greater extent of muscle loss over the longer time period. Furthermore, the other study did not specify whether the subjects had spastic and/or flaccid paralysis, which may have affected the results (Wilmet et al. 1995) (Coupaud et al. 2009) (Eser, Frotzler, Zehnder, Schiessl & Denoth 2005).

The results of this study found similar increases in fat following SCI as compared to other related studies. At 3-months post-SCI, Gorgey & Dudley (2006) found an increase in fat of 26%. Similarly, in this study, Table 5.1 shows an increase in fat of $12.1\% \pm 23.8$ after 4-months. Once again, the slight differences can be likely attributed to both the variable timings of scans following injury and the paralysis type (i.e., spastic or flaccid).

Eser et al. (2004) found that cortical bone had approximately a 30% smaller CSA in the tibia in chronic SCI, nearly 8 years following immobilisation due to SCI. Table 5.1 indicates that cortical bone decreases by $2.5\% \pm 2.3$ after 12-months following SCI, indicating the cortical bone CSA is beginning to decrease over time.

Despite these predictable changes, Table 5.1 (variable thresholding) also indicates a high variability in the changes of soft tissue and bone in the pQCT scans. Although most images produced typical results, several subjects showed unexpected changes, especially with respect to changes in their soft tissue quantity. There are several possible explanations for these atypical results.

- Due to spasticity of the muscles in some patients, movement artefact was present in some of the images. An example of this effect can be seen in the baseline and T4 images of Figure 5.8. In several cases, this movement artefact severely degraded the quality of these images, and density values within the images were strongly affected. In these images, streaks within the image are present, artificially increasing the density values along that region. This especially affected the soft tissue, and so the quantity of muscle detected by the software may have been larger than expected in images with movement artefact.

- There may be visible differences in soft tissue quantities between subjects dependent on whether they had spastic or flaccid paralysis. Because the muscles experienced involuntary movements and spasms, the muscles still received stimulation. Thus, these patients may not have experienced as high a degree of muscular atrophy following SCI as those who had flaccid paralysis. In this study, 15 of the 18 patients had spastic paralysis, while only 3 had fully flaccid paralysis. The subject presented in Section 5.2.1

experienced flaccid SCI, and thus may explain why he had such visible muscular atrophy during the first 12 months post-SCI. Conversely, the subjects presented in Section 5.2.2 and Section 5.2.3 both had spastic paralysis. This heightened muscular atrophy in patients with flaccid SCI would be consistent with other studies performed by Wilmet et al. (1995), Coupaud et al. (2009), and Eser, Frotzler, Zehnder, Schiessl & Denoth (2005).

- The use of pressure stockings by the subjects may have affected the total cross-sectional area of the leg in the images. For several of the scans, the subjects wore pressure stockings. However, the use of pressure stockings was not consistent subject-to-subject, or between scans for a single subject. This may have affected the cross-sectional area if the soft tissue in the leg, reducing muscle and fat cross-sectional area when the pressure stocking was being worn. For example, a pressure stocking was being worn by the subject exemplified in Section 5.2.3 during the baseline scan, but not during any of the remaining three scans. This may explain why the muscle cross-sectional area at the baseline scan appeared to be significantly less than at T2, T3, or T4.

- Spinal shock may have also had an effect on the muscle changes seen in the subject described in Section 5.2.3. Spinal shock is an effect seen in many SCI patients, usually within their first month post-injury. During this phenomenon, they experience a temporary loss in all or most motor or sensory function below the level of their injury (Atkinson & Atkinson 1996). As a result, patients who will eventually develop spastic paralysis may experience several weeks of flaccid paralysis during the acute phase of SCI. In the case of the subject in Section 5.2.3, the patient may have suffered spinal shock during which the muscle would have atrophied quickly in bedrest prior to the baseline scan. When the spasms and movements associated with spastic

paralysis presented, the leg could have seen an overall increase in muscle mass between the baseline scan and T2 due to muscle stimulation.

- As discussed previously, changes in muscle quality usually lead to changes in CT attenuation values (Goodpaster et al. 2000). In this study, the density threshold between fat and muscle was held constant for each subject for all four scans. Under the assumption that muscle tissue density would not change significantly over the 12 month period, averaging the calculated thresholds was aimed at reducing error within the calculated value. Although this methodology is improved over the universal constant threshold, the calculated threshold for images may need to by adjusted for each individual scan to account for reduced quality in muscle tissue.

- Though it is useful in finding bone properties, pQCT is not always suited to measuring the quantity of soft tissue *in vivo* with a high level of accuracy. In particular, it loses some degree of accuracy when measuring muscle tissue with a high lipid content (Schick et al. 2002), whereas MRI is able to better segment the tissues. Ideally, pQCT imaging could be used in parallel with another imaging technique to compare pQCT-derived bone measurements with soft tissue measurements from MRI.

The main objective in this study was to characterise the relationships between muscle atrophy and bone loss following complete paralysis of the lower limbs. To accomplish this, two separate studies were performed. Within the first study, the total muscle CSA loss that had occurred 4 months post-injury was compared to the total cortical bone CSA loss that had occurred 12 months post-injury. As described in Chapter 2, the diaphysis of the tibia is mostly composed of cortical bone, and thus experiences the largest levels of bone loss within the shaft. This thinning of the cortical wall is most easily identified by a change in cortical CSA (Biering-Sorensen et al. 1990). The first study's comparison resulted

in a positive linear relationship between $\Delta CSA_{muscle,T2}$ and $\Delta CSA_{cortical,T4}$ ($r = 0.27$). However, this value was determined the be insignificant for the population size ($p = 0.51$).

The second study performed was the comparison of the total muscle CSA loss that had occurred 4 months post-injury to the total trabecular bone density loss within the proximal epiphysis of the tibia at 12 months post-injury. Trabecular bone responds much more quickly to changes in bone metabolism and thus sees the first and most dramatic effects of disuse osteoporosis (Wilmet et al. 1995). This particular bone loss is seen through changes in bone mineral density (Biering-Sorensen et al. 1990). However, a negligible and weak positive correlation ($r = 0.02$, $p = 0.53$) was found between muscle loss and trabecular bone loss.

Chapter 7

Conclusions and

Recommendations for Future

Work

The overall aim of this project was to identify whether there was a relationship between early muscle loss following paralysis and future bone loss. This was accomplished through the use of pQCT image scans of the lower leg, obtained from subjects at several different time points following a spinal cord injury. These scans were analysed through the use of software that was developed in Matlab, which was able to automatically segment the images into tissue components. The software could then identify the quantities of fat, muscle, and bone present in each scan, which could then be used to study relationships in soft tissue and bone changes over time.

The software that was developed used a novel technique that identified the density threshold between fat and muscle from within pQCT images. Overall, variable thresholding was the preferred technique in identifying muscle and fat tissue. This methodology was able to account for changes in muscle quality that can accompany disuse-related atrophy, such as increased intercellular lipid content. Further work in developing a tool that can calculate separate thresholds for each scan accurately is advised to alleviate concerns over large changes in muscle quality for a single subject during the first 12 months post-SCI.

Analysis of the data indicated that there was a positive correlation between change in muscle and change in bone; however, this relationship was not found to be statistically significant. To further this study, it may be useful to analyse pQCT scans from different parts of the leg. Femur images have a higher resolution (0.3 mm voxel edge length, compared to 0.5 mm voxel edge length for the tibia), and the higher resolution of these scans provides the ability to distinguish between different muscle groups. Thus, changes in muscle and intramuscular/subcutaneous fat may be more visible and easily segmented. These data could then be compared to the changes in cross-sectional area of the tibial diaphysis, changes in the

bone mineral density of the tibial epiphyses, and changes in the cross-sectional area of the femur diaphysis.

Alternatively, the use of other imaging devices may improve the accuracy of this study with respect to soft tissue. The use of pQCT in measuring bone geometric properties and BMD is advocated, as this imaging technique is able to accurately and precisely identify changes in both cortical and trabecular bone. However, muscle and other soft tissue can be more accurately defined through MRI. MRI is enhances the ability to distinguish high lipid content. In turn, this could improve the ability to calculate an appropriate threshold for skeletal muscle.

It may be further advantageous to study the geometric changes in the bone structure during the 12-month period post-SCI. As discussed in Chapter 2, the cortical bone shell becomes thinner as a result of disuse osteoporosis (Eser et al. 2004). Therefore, a study in the changes of cortical bone structure could be compared to change in muscle cross-sectional area, with the aim of determining if a relationship exists between these two figures.

Overall, this study outlined the possibility for developing a relationship between early muscle atrophy following SCI and future bone loss. Ideally, this relationship could be developed to be used clinically in SCI patients. If a patient were to present with high levels of muscle atrophy within the first several months following SCI, this would be an indication that he is especially susceptible to bone loss and thus require earlier and more intensive interventions. Given the morbidity and mortality associated with fracture following bone loss in SCI patients, further work on this subject would provide a critical tool in improving the outlook of these patients with respect to osteoporosis progression and fracture risk.

Appendix A
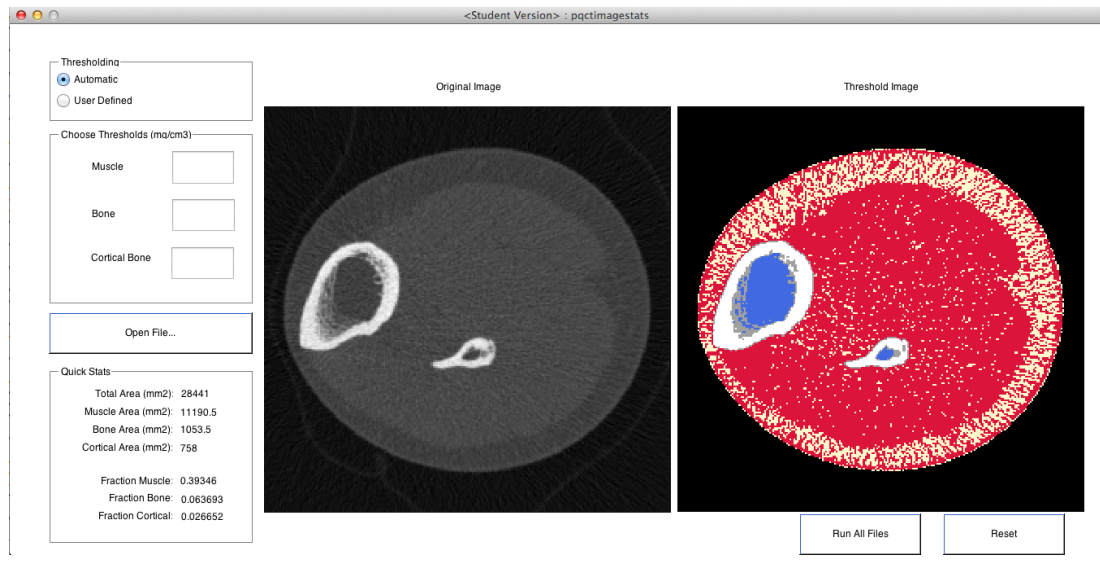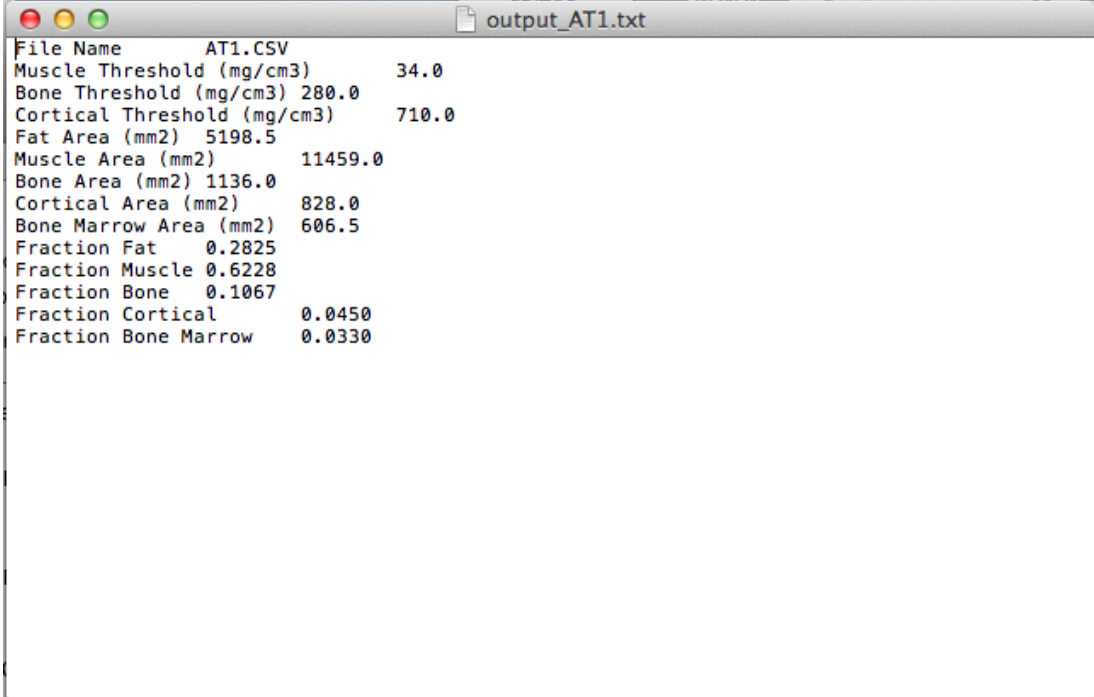
Matlab Code

A.1   Graphical User Interface

FIGURE A.1: Sample screenshot of Graphical User Interface (GUI)

A.2   GUI Output

A.2.1   General Output

By selecting "Open File..." within the GUI, a specific CSV image file can be evaluated, which outputs a tab-delimited text file, as demonstrated in Figure A.2.


```
output_AT1.txt
File Name        AT1.CSV
Muscle Threshold (mg/cm3)       34.0
Bone Threshold (mg/cm3) 280.0
Cortical Threshold (mg/cm3)     710.0
Fat Area (mm2)  5198.5
Muscle Area (mm2)       11459.0
Bone Area (mm2) 1136.0
Cortical Area (mm2)     828.0
Bone Marrow Area (mm2)  606.5
Fraction Fat    0.2825
Fraction Muscle 0.6228
Fraction Bone   0.1067
Fraction Cortical       0.0450
Fraction Bone Marrow    0.0330
```

FIGURE A.2: Sample output from GUI

A.2.2 "Run All Files" Function Output

Alternatively, by selecting "Run All Files" within the GUI, all CSV image files within the folder will be run. A sample of this is seen in Figure A.3.

FIGURE A.3: Sample all files output from GUI

A.3   pqctimagestats.m

```matlab
function varargout = pqctimagestats(varargin)

%% Begin initialization code
gui_Singleton = 1;
gui_State = struct('gui_Name',       mfilename, ...
                   'gui_Singleton',  gui_Singleton, ...
                   'gui_OpeningFcn', @pqctimagestats_OpeningFcn, ...
                   'gui_OutputFcn',  @pqctimagestats_OutputFcn, ...
                   'gui_LayoutFcn',  [] , ...
                   'gui_Callback',   []);
if nargin && ischar(varargin{1})
    gui_State.gui_Callback = str2func(varargin{1});
end

if nargout
    [varargout{1:nargout}] = gui_mainfcn(gui_State, varargin{:});
else
    gui_mainfcn(gui_State, varargin{:});
end

%% Executes just before pqctimagestats is made visible
function pqctimagestats_OpeningFcn(hObject, eventdata, handles, varargin)
handles.output = hObject;
guidata(hObject, handles);
clc

%% Outputs from this function are returned to the command line
function varargout = pqctimagestats_OutputFcn(hObject, eventdata, handles)
varargout{1} = handles.output;

%% --- Executes when selected object is changed in uipanel4.
```

```matlab
function uipanel4_SelectionChangeFcn(hObject, eventdata, handles)
rb = get(eventdata.NewValue,'Tag');
handles.rb = rb;
guidata(hObject, handles);


%% Muscle threshold text box
function threshold_muscle_textbox_Callback(hObject, eventdata, handles)
handles.threshold_muscle = str2double(get(hObject,'String'));
guidata(hObject, handles);


function threshold_muscle_textbox_CreateFcn(hObject, eventdata, handles)
if ispc && isequal(get(hObject,'BackgroundColor'),...
    get(0,'defaultUicontrolBackgroundColor'))
    set(hObject,'BackgroundColor','white');
end


%% Bone threshold text box
function threshold_bone_textbox_Callback(hObject, eventdata, handles)
handles.threshold_bone = str2double(get(hObject,'String'));
guidata(hObject, handles);


function threshold_bone_textbox_CreateFcn(hObject, eventdata, handles)
if ispc && isequal(get(hObject,'BackgroundColor'),...
    get(0,'defaultUicontrolBackgroundColor'))
    set(hObject,'BackgroundColor','white');
end


%% Cortical bone threshold text box
function threshold_cortical_textbox_Callback(hObject, eventdata, handles)
handles.threshold_cortical = str2double(get(hObject,'String'));
guidata(hObject, handles)


function threshold_cortical_textbox_CreateFcn(hObject, eventdata, handles)
if ispc && isequal(get(hObject,'BackgroundColor'),...
```

```matlab
    get(0,'defaultUicontrolBackgroundColor'))
    set(hObject,'BackgroundColor','white');
end


%% Open file push button
function getfile_Callback(hObject, eventdata, handles)
[filename,filepath]=uigetfile({'*.csv','All Files'},...
  'Select Data File 1');
  cd(filepath);
if isfield(handles,'rb');
    rb = handles.rb;
else
    rb = 'auto_thresholds';
end
if strcmp(rb,'user_thresholds') == 1;
    threshold_muscle = handles.threshold_muscle;
    threshold_bone = handles.threshold_bone;
    threshold_cortical = handles.threshold_cortical;
else
    threshold_muscle = NaN;
    threshold_bone = NaN;
    threshold_cortical = NaN;
end
[I_original,I_colour,fulloutputstats] = ...
    pqctimagefunction(filename,threshold_muscle,...
    threshold_bone,threshold_cortical);
imshow(I_original,'Parent',handles.axes1);
imshow(I_colour,'Parent',handles.axes2);
area_xsection = num2str(fulloutputstats(4));
area_muscle = num2str(fulloutputstats(6));
area_bone = num2str(fulloutputstats(7));
area_cortical = num2str(fulloutputstats(8));
fraction_muscle = num2str(fulloutputstats(11));
fraction_bone = num2str(fulloutputstats(12));
```

```matlab
fraction_cortical = num2str(fulloutputstats(13));
set(handles.outputtext1,'String',area_xsection)
set(handles.outputtext2,'String',area_muscle)
set(handles.outputtext3,'String',area_bone)
set(handles.outputtext5,'String',fraction_muscle)
set(handles.outputtext6,'String',fraction_bone)
set(handles.outputtext4,'String',area_cortical)
set(handles.outputtext7,'String',fraction_cortical)

%% Run all files push button
function runallfiles_Callback(hObject, eventdata, handles)
if exist('output_allfiles.csv', 'file') == 2
  delete('output_allfiles.csv');
end
files = dir('*.csv');
for d = 1:length(files)
    filename = fullfile(files(d).name);
    ind_filename = strfind(filename,'._');
    if isempty(ind_filename);
        if isfield(handles,'rb');
            rb = handles.rb;
        else
            rb = 'auto_thresholds';
        end
        if strcmp(rb,'user_thresholds') == 1;
            threshold_muscle = handles.threshold_muscle;
            threshold_bone = handles.threshold_bone;
            threshold_cortical = handles.threshold_cortical;
        else
            threshold_muscle = NaN;
            threshold_bone = NaN;
            threshold_cortical = NaN;
        end
        [~,~,fulloutputstats] = pqctimagefunction(filename,threshold_muscle,...
```

```matlab
            threshold_bone,threshold_cortical);
        fulloutputstats=num2cell(fulloutputstats,length(fulloutputstats));
        fulloutputstats = [cellstr(filename) fulloutputstats];
        fulloutputstats_allfiles(1,:) = {'File' 'Muscle Threshold' ...
            'Bone Threshold' 'Cortical Threshold' 'Total Area (mm2)' ...
            'Fat Area (mm2)' 'Muscle Area (mm2)' 'Bone Area (mm2)' ...
            'Cortical Area (mm2)' 'Bone Marrow Area (mm2)' ...
            'Fraction Fat' 'Fraction Muscle' 'Fraction Bone' ...
            'Fraction Cortical' 'Fraction Bone Marrow'};

        fulloutputstats_allfiles(size(fulloutputstats_allfiles,1)+1,:) = ...
            fulloutputstats;
    end
end
fid=fopen('output_allfiles.csv','w');
for i=1:size(fulloutputstats_allfiles,1)
    if i == 1
        fprintf(fid,'%s,%s,%s,%s,%s,%s,%s,%s,%s,%s,%s,%s,%s,%s,%s\n',...
            fulloutputstats_allfiles{i,:});
    else
        fprintf(fid,'%s,%f,%f,%f,%f,%f,%f,%f,%f,%f,%f,%f,%f,%f,%f\n',...
            fulloutputstats_allfiles{i,:});
    end
end
fclose(fid);

%% Reset push button
function resetbutton_Callback(hObject, eventdata, handles)
close(gcbf)
pqctimagestats
```

A.4   pqctimagefunction.m

```matlab
function [I_original,I_colour,fulloutputstats] =...
    pqctimagefunction(filename,threshold_muscled,...
    threshold_boned,threshold_corticald)


%% Read input file
inputfile = dlmread(filename,';');


%% Normalise input file (0 to 1) & show original image
I_original = mat2gray(inputfile,[min(inputfile(:)) max(inputfile(:))]);


%% Filter out stray artifacts
BW = im2bw(I_original,.2);
BW = imfill(BW,'holes');
BW = bwareaopen(BW,5000);
I_final = I_original;
I_final(imcomplement(BW)) = 0;


%% Determine & normalise threshold values (0 to 1)
if isnan(threshold_muscled) == 1;
    threshold_boned = 280;
    threshold_corticald = 710;
    gaussian_filter = fspecial('gaussian',[12 12],0.5);
    I_filtered = imfilter(I_final,gaussian_filter,'replicate');
    [counts,x] = imhist(I_filtered,256*5);
    counts(1,:) = 0;
    histogram_filtered = sgolayfilt(counts,3,11);
    dcounts = diff(histogram_filtered)./diff((1:256*5)');
    dir = diff(sign(dcounts));
    [dirrow,~] = find(dir>0);
    poly = polyfit([0 1],[min(inputfile(:)) max(inputfile(:))],1);
    mindensity = 0;
```

```matlab
        mindensity = (((mindensity+341)/1.495)-poly(2))/poly(1);
        for i = 1:length(dirrow)
            if x(dirrow(i)) > mindensity
                threshold_muscle = x(dirrow(i)+1);
                break
            end
        end
        threshold_muscled = poly(1)*threshold_muscle+poly(2);
        threshold_muscled = threshold_muscled*1.495-341;
    else
        threshold_muscle = (threshold_muscled+341)/1.495;
        threshold_muscle = mat2gray(threshold_muscle,...
            [min(inputfile(:)) max(inputfile(:))]);
    end
    threshold_bone = (threshold_boned+341)/1.495;
    threshold_bone = mat2gray(threshold_bone,...
        [min(inputfile(:)) max(inputfile(:))]);
    threshold_cortical = (threshold_corticald+341)/1.495;
    threshold_cortical = mat2gray(threshold_cortical,...
        [min(inputfile(:)) max(inputfile(:))]);

    %% Extract bone tissue as binary
    I_bone = I_final >= threshold_bone;

    %% Filter out inner bone (marrow)
    I_final2 = I_bone;
    [~,threshold] = edge(I_final2,'sobel');
    fudgefactor = 1;
    BWbone1 = edge(I_final2,'sobel',threshold*fudgefactor);
    se90 = strel('line',2,90);
    se0 = strel('line',2,0);
    BWbone2 = imdilate(BWbone1,[se90 se0]);
    BWbone3 = imfill(BWbone2,'holes');
    seD = strel('diamond',3);
```

```matlab
BWbone4 = imerode(BWbone3,seD);
BWbone4 = imerode(BWbone4,seD);
BWbone_final = imfill(BWbone4,'holes');


%% Extract tissue types as binaries
I_marrow = BWbone_final.*imcomplement(I_bone);
if not(isnan(threshold_corticald))
    I_trabecular = I_final >= threshold_bone & I_final < threshold_cortical;
    I_cortical = I_final >= threshold_cortical;
end
I_muscle = I_final >= threshold_muscle & I_final < threshold_bone;
I_muscle = I_muscle.*imcomplement(BWbone_final);
I_fat = I_final < threshold_muscle & I_final > 0;
I_fat = I_fat.*imcomplement(BWbone_final);


%% Find areas of each tissue
size_xsection = isfinite(I_final);
area_xsection = sum(size_xsection(:) == 1);
area_xsection = area_xsection*0.5;
if not(isnan(threshold_corticald))
    area_bone = sum(I_trabecular(:) == 1)+sum(I_cortical(:) == 1);
    area_bone = area_bone*0.5;
    area_cortical = sum(I_cortical(:) == 1);
    area_cortical = area_cortical*0.5;
    fraction_bone = (area_bone+area_cortical)/area_xsection;
    fraction_cortical = area_cortical/area_xsection;
else
    area_bone = sum(I_bone(:) == 1);
    area_bone = area_bone*0.5;
    fraction_bone = area_bone/area_xsection;
    area_cortical = NaN;
    fraction_cortical = NaN;
end
area_muscle = sum(I_muscle(:) == 1);
```

```matlab
area_muscle = area_muscle*0.5;
fraction_muscle = area_muscle/area_xsection;
area_marrow = sum(I_marrow(:) == 1);
area_marrow = area_marrow*0.5;
fraction_marrow = area_marrow/area_xsection;
area_fat = sum(I_fat(:) == 1);
area_fat = area_fat*0.5;
fraction_fat = area_fat/area_xsection;


%% Create colourised image
I_colour = repmat({NaN},[size(I_final),3]);
for i = 1:size(I_final,1)
    for j = 1:size(I_final,2)
        if I_fat(i,j) == 1
            I_colour(i,j,:) = {1 250/255 205/255};
        end
        if I_muscle(i,j) == 1
            I_colour(i,j,:) = {220/255 20/255 60/255};
        end
        if I_marrow(i,j) == 1
            I_colour(i,j,:) = {65/255 105/255 225/255};
        end
        if not(isnan(threshold_corticald))
            if I_trabecular(i,j) == 1
                I_colour(i,j,:) = {160/255 160/255 160/255};
            end
            if I_cortical(i,j) == 1
                I_colour(i,j,:) = {1 1 1};
            end
        else
            if I_bone(i,j) == 1
                I_colour(i,j,:) = {1 1 1};
            end
        end
```

```matlab
        end
end
I_colour = cell2mat(I_colour);

%% Generate full result matrix
fulloutputstats = [threshold_muscled,...
    threshold_boned,...
    threshold_corticald,...
    area_xsection,...
    area_fat,...
    area_muscle,...
    area_bone,...
    area_cortical,...
    area_marrow,...
    fraction_fat,...
    fraction_muscle,...
    fraction_bone,...
    fraction_cortical,...
    fraction_marrow];
```

Bibliography

A.D.A.M., Inc. (2013), 'Osteoporosis in-depth report'.
  URL: *http://www.nytimes.com/health/guides/disease/osteoporosis/print.html*

Atkinson, P. & Atkinson, J. (1996), 'Spinal shock', *Mayo Clinic Proceedings* **71**(4), 384–389.

Bartl, R. & Frisch, B. (2009), Bone density in osteoporosis, *in* 'Osteoporosis', Springer Berlin Heidelberg, pp. 63–73.

Biering-Sorensen, F., Bohr, H. & Schaadt, O. (1990), 'Longitudinal study of bone mineral content in the lumbar spine, the forearm and the lower extremities after spinal cord injury.', *European Journal of Clinical Investigation* **20**(3), 330–335.

Blake, G. & Fogelman, I. (2007), 'The role of DXA bone density scans in the diagnosis and treatment of osteoporosis', *Postgraduate Medical Journal* **83**(982), 509–517.

Bland, J. & Altman, D. (1986), 'Statistical methods for assessing agreement between two methods of clinical measurement', *Lancet* **327**(8476), 307–310.

Bolotin, H. (2007), 'DXA in vivo BMD methodology: an erroneous and misleading research and clinical gauge of bone mineral status, bone fragility, and bone remodelling', *Bone* **41**(1), 138–154.

Bonnick, S. & Lewis, L. (2006), *Bone Densitometry for Technologists*, 2 edn, Humana Press, Totowa, NJ.

Bono, C. & Einhorn, T. (2003), 'Overview of osteoporosis: pathophysiology and determinants of bone strength', *European Spine Journal* **12 Suppl 2**, S90–S96.

Boonyarom, O. & Inui, K. (2006), 'Atrophy and hypertrophy of skeletal muscles: structural and functional aspects', *Acta Physiologica* **188**(2), 77–89.

Brandi, M. (2009), 'Microarchitecture, the key to bone quality', *Rheumatology* **48 Suppl 4**, iv3–8.

Braun, M., Meta, M., Schneider, P. & Reiners, C. (1998), 'Clinical evaluation of a high-resolution new peripheral quantitative computerized tomography (pQCT) scanner for the bone densitometry at the lower limbs', *Physics in Medicine and Biology* **43**(8), 2279.

Calmels, P., Vico, L., Alexandre, C. & Minaire, P. (1995), 'Cross-sectional study of muscle strength and bone mineral density in a population of 106 women between the ages of 44 and 87 years: relationship with age and menopause', *European Journal of Applied Physiology and Occupational Physiology* **70**(2), 180–186.

Castro, M., Apple, Jr., D., Hillegass, E. & Dudley, G. (1999), 'Influence of complete spinal cord injury on skeletal muscle cross-sectional area within the first 6 months of injury', *European Journal of Applied Physiology and Occupational Physiology* **80**(4), 373–378.

Centers for Disease Control and Prevention (2010), 'Spinal cord injury (SCI): Fact sheet'.
URL: *http://www.cdc.gov/traumaticbraininjury/scifacts.html*

Coupaud, S., McLean, A. & Allan, D. (2009), 'Role of peripheral quantitative computed tomography in identifying disuse osteoporosis in paraplegia', *Skeletal Radiology* **38**(10), 989–995.

Cowin, S., ed. (2001), *Bone Mechanics Handbook*, 2 edn, CRC Press, Boca Raton, FL.

Dougherty, G. (2009), *Digital Image Processing for Medical Applications*, Cambridge University Press, Cambridge, UK.

Elder, C. P., Apple, D., Bickel, C., Meyer, R. & Dudley, G. (2004), 'Intramuscular fat and glucose tolerance after spinal cord injury a cross-sectional study', *Spinal Cord* **42**(12), 711–716.

Engelke, K., Adams, J., Armbrecht, G., Augat, P., Bogado, C., Bouxsein, M., Felsenberg, D., Ito, M., Prevrhal, S., Hans, D. & Lewiecki, E. (2008), 'Clinical use of quantitative computed tomography and peripheral quantitative computed tomography in the management of osteoporosis in adults: the 2007 ISCD official positions', *Journal of Clinical Densitometry* **11**(1), 123–162.

Eser, P., Frotzler, A., Zehnder, Y. & Denoth, J. (2005), 'Fracture threshold in the femur and tibia of people with spinal cord injury as determined by peripheral quantitative computed tomography', *Archives of Physical Medicine and Rehabilitation* **86**(3), 498–504.

Eser, P., Frotzler, A., Zehnder, Y., Schiessl, H. & Denoth, J. (2005), 'Assessment of anthropometric, systemic, and lifestyle factors influencing bone status in the legs of spinal cord injured individuals', *Osteoporosis International* **16**(1), 26–34.

Eser, P., Frotzler, A., Zehnder, Y., Wick, L., Knecht, H., Denoth, J. & Schiessl, H. (2004), 'Relationship between the duration of paralysis and bone structure: a pQCT study of spinal cord injured individuals', *Bone* **34**(5), 869–880.

Findlay, C. (2012), Image analysis tool for the characterisation of bone turnover in the appendicular skeleton, PhD thesis, University of Glasgow, Glasgow, UK.

Freehafer, A., Hazel, C. & Becker, C. (1981), 'Lower extremity fractures in patients with spinal cord injury', *Paraplegia* **19**(6), 367–372.

Frost, H. (2004), *The Utah Paradigm of Skeletal Physiology: Bone and bones and associated problems*, Vol. 1, International Society of Musculoskeletal and Neuronal Interactions, Greece.

Frost, H. M. (1994), 'Wolff's law and bone's structural adaptations to mechanical usage: an overview for clinicians', *The Angle orthodontist* **64**(3), 175–188.

Giangregorio, L. & McCartney, N. (2006), 'Bone loss and muscle atrophy in spinal cord injury: epidemiology, fracture prediction, and rehabilitation strategies', *The Journal of Spinal Cord Medicine* **29**(5), 489–500.

Goodpaster, B., Carlson, C., Visser, M., Kelley, D., Scherzinger, A., Harris, T., Stamm, E. & Newman, A. (2001), 'Attenuation of skeletal muscle and strength in the elderly: the health ABC study', *Journal of Applied Physiology* **90**(6), 2157–2165.

Goodpaster, B., Kelley, D., Thaete, F., He, J. & Ross, R. (2000), 'Skeletal muscle attenuation determined by computed tomography is associated with skeletal muscle lipid content', *Journal of Applied Physiology* **89**(1), 104–110.

Gorgey, A. & Dudley, G. (2006), 'Skeletal muscle atrophy and increased intramuscular fat after incomplete spinal cord injury', *Spinal Cord* **45**(4), 304–309.

Hadjidakis, D. & Androulakis, I. (2006), 'Bone remodeling', *Annals of the New York Academy of Sciences* **1092**(1), 385–396.

Hong, J., Hipp, J., Mulkern, R., Jaramillo, D. & Snyder, B. (2000), 'Magnetic resonance imaging measurements of bone density and cross-sectional geometry', *Calcified Tissue International* **66**(1), 74–78.

Hudelmaier, M., Kuhn, V., Lochmller, E., Well, H., Priemel, M., Link, T. & Eckstein, F. (2004), 'Can geometry-based parameters from pQCT and material parameters from quantitative ultrasound (QUS) improve the prediction of radial bone strength over that by bone mass (DXA)?', *Osteoporosis International* **15**(5), 375–381.

Jacobs, P. & Nash, M. (2004), 'Exercise recommendations for individuals with spinal cord injury', *Sports Medicine* **34**(11), 727–751.

Kasper, C., Talbot, L. & Gaines, J. (2002), 'Skeletal muscle damage and recovery', *AACN Clinical Issues* **13**(2), 237–247.

Lau, R. & Guo, X. (2011), 'A review on current osteoporosis research: With special focus on disuse bone loss', *Journal of Osteoporosis* **2011**.

Lazo, M., Shirazi, P., Sam, M., Giobbie-Hurder, A., Blacconiere, M. & Muppidi, M. (2001), 'Osteoporosis and risk of fracture in men with spinal cord injury', *Spinal Cord* **39**(4), 208.

Lu, T.-W., Taylor, S., O'Connor, J. & Walker, P. (1997), 'Influence of muscle activity on the forces in the femur: an in vivo study', *Journal of Biomechanics* **30**(1112), 1101–1106.

MacIntosh, B., Gardiner, P. & McComas, A. (2005), *Skeletal Muscle: Form and Function*, 2 edn, Human Kinetics.

Martini, F., Nath, J. & Bartholomew, E. (2011), *Fundamentals of Anatomy & Physiology*, 9 edn, Benjamin Cummings, San Francisco.

Maynard, Jr., F., Bracken, M., Creasey, G., Ditunno, Jr., J., Donovan, W., Ducker, T., Garber, S., Marino, R., Stover, S., Tator, C., Waters, R., Wilberger, J. & Young, W. (1997), 'International standards for neurological and functional classification of spinal cord injury. american spinal injury association', *Spinal Cord* **35**(5), 266–274.

McKinley, W., Jackson, A., Cardenas, D. & De Vivo, M. (1999), 'Long-term medical complications after traumatic spinal cord injury: a regional model systems analysis', *Archives of Physical Medicine and Rehabilitation* **80**(11), 1402–1410.

Mikla, V. & Mikla, V. (2013), *Medical Imaging Technology*, 1 edn, Elsevier.

Mitsiopoulos, N., Baumgartner, R., Heymsfield, S., Lyons, W., Gallagher, D. & Ross, R. (1998), 'Cadaver validation of skeletal muscle measurement by magnetic resonance imaging and computerized tomography', *Journal of Applied Physiology* **85**(1), 115–122.

National Institutes of Health (2012), 'Osteoporosis overview'.
URL: *http://www.niams.nih.gov/HealthInfo/Bone/Osteoporosis/overview.asp*

National Osteoporosis Society (2013), 'Scans and tests and osteoporosis'.
URL: *http://www.nos.org.uk/NetCommunity/Document.doc?id=388*

Neri, E., Caramella, D., Bartolozzi, C. & Baert, A. (2007), *Image Processing in Radiology: Current Applications*, 2008 edn, Springer, Berlin.

Rittweger, J., Beller, G., Ehrig, J., Jung, C., Koch, U., Ramolla, J., Schmidt, F., Newitt, D., Majumdar, S., Schiessl, H. & Felsenberg, D. (2000), 'Bone-muscle strength indices for the human lower leg', *Bone* **27**(2), 319–326.

Schafer, R. (2011), 'What is a savitzky-golay filter?', *IEEE Signal Processing Magazine* **28**(4), 111–117.

Schantz, P., Randall-Fox, E., Hutchison, W., Tydn, A. & Astrand, P. (1983), 'Muscle fibre type distribution, muscle cross-sectional area and maximal voluntary strength in humans', *Acta Physiologica Scandinavica* **117**(2), 219–226.

Schick, F., Machann, J., Brechtel, K., Strempfer, A., Klumpp, B., Stein, D. & Jacob, S. (2002), 'MRI of muscular fat', *Magnetic Resonance in Medicine* **47**(4), 720–727.

Schiessl, H. & Willnecker, J. (1998), Muscle cross sectional area and bone cross sectional area in the human lower leg measured with peripheral computed tomography, *in* G. Lyritis, ed., 'Musculoskeletal Interactions', Vol. 2, Holonome Editions, Athens, pp. 47–52.

Sinaki, M., McPhee, M., Hodgson, S., Merritt, J. & Offord, K. (1986), 'Relationship between bone mineral density of spine and strength of back extensors in healthy postmenopausal women', *Mayo Clinic Proceedings* **61**(2), 116–122.

Takata, S. & Yasui, N. (2001), 'Disuse osteoporosis', *The Journal of Medical Investigation* **48**(3-4), 147–156.

Tucker, G., Metcalfe, A., Pearce, C., Need, A., Dick, I., Prince, R. & Nordin, B. (2007), 'The importance of calculating absolute rather than relative fracture risk', *Bone* **41**(6), 937–941.

Van De Graaff, K., Rhees, R. & Palmer, S. (2010), *Schaum's Outline of Human Anatomy and Physiology*, 3 edn, McGraw Hill, New York.

Vestergaard, P., Krogh, K., Rejnmark, L. & Mosekilde, L. (1998), 'Fracture rates and risk factors for fractures in patients with spinal cord injury', *Spinal Cord* **36**(11), 790.

Vico, L., Collet, P., Guignandon, A., Lafage-Proust, M., Thomas, T., Rehaillia, M. & Alexandre, C. (2000), 'Effects of long-term microgravity exposure on cancellous and cortical weight-bearing bones of cosmonauts', *Lancet* **355**(9215), 1607–1611.

Wilmet, E., Ismail, A., Heilporn, A., Welraeds, D. & Bergmann, P. (1995), 'Longitudinal study of the bone mineral content and of soft tissue composition after spinal cord section', *Paraplegia* **33**(11), 674–677.

Wyndaele, M. & Wyndaele, J.-J. (2006), 'Incidence, prevalence and epidemiology of spinal cord injury: what learns a worldwide literature survey?', *Spinal Cord* **44**(9), 523–529.

Yu, E., Thomas, B., Brown, J. & Finkelstein, J. (2012), 'Simulated increases in body fat and errors in bone mineral density measurements by DXA and QCT', *Journal of Bone and Mineral Research* **27**(1), 119–124.

Zimmermann, C., Smidt, G., Brooks, J., Kinsey, W. & Eekhoff, T. (1990), 'Relationship of extremity muscle torque and bone mineral density in postmenopausal women', *Physical Therapy* **70**(5), 302–309.